Article

Cell

Phosphorylation-Mediated IFN-γR2 Membrane Translocation Is Required to Activate Macrophage Innate Response

Graphical Abstract

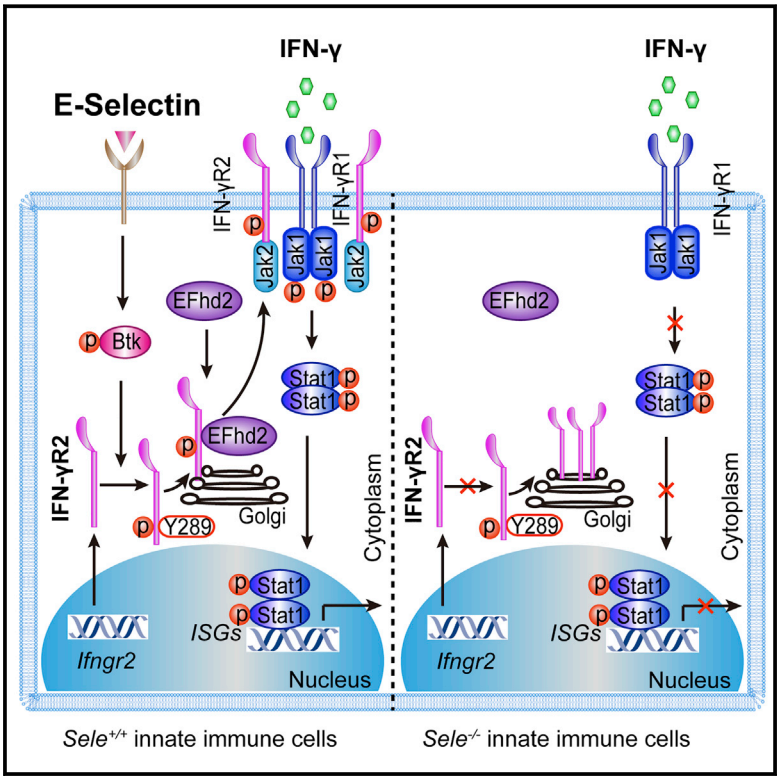

Highlights

- E-selectin promotes macrophage activation by increasing IFN-γR2 membrane expression
- Extrinsic E-selectin enhances macrophage IFN-γR2 membrane translocation from Golgi
- IFN-γR2 phosphorylation by BTK and binding of EFhd2 facilitates its translocation
- Assembly of functional cytokine receptors enables cytokine functions in immunity

Authors

Xiaoqing Xu, Jia Xu, Jiacheng Wu, ..., Juan Liu, Bing Liu, Xuetao Cao

Correspondence

caoxt@immunol.org

In Brief

Membrane translocation of cytoplasmic IFN-γR2 is a critical step for the activation of macrophage innate response against intracellular bacterial infection.

Xu et al., 2018, Cell *175*, 1–16
November 29, 2018
https://doi.org/10.1016/j.cell.2018.09.011

CellPress

Please cite this article in press as: Xu et al., Phosphorylation-Mediated IFN-γR2 Membrane Translocation Is Required to Activate Macrophage Innate Response, Cell (2018), https://doi.org/10.1016/j.cell.2018.09.011

Article

Cell

Phosphorylation-Mediated IFN-γR2 Membrane Translocation Is Required to Activate Macrophage Innate Response

Xiaoqing Xu,[1,2] Jia Xu,[1] Jiacheng Wu,[1] Ye Hu,[1] Yanmei Han,[2] Yan Gu,[2] Kai Zhao,[1] Qian Zhang,[2] Xingguang Liu,[2] Juan Liu,[2] Bing Liu,[3] and Xuetao Cao[1,2,4,5,*]

[1]Department of Immunology and Center for Immunotherapy, Institute of Basic Medical Sciences, Peking Union Medical College, Chinese Academy of Medical Sciences, 100005 Beijing, China

[2]National Key Laboratory of Medical Immunology and Institute of Immunology, Second Military Medical University, 200433 Shanghai, China

[3]Translational Medicine Center, Academy of Military Medical Sciences, 100024 Beijing, China

[4]College of Life Science, Nankai University, 300071 Tianjin, China

[5]Lead Contact

*Correspondence: caoxt@immunol.org

https://doi.org/10.1016/j.cell.2018.09.011

SUMMARY

As a critical step during innate response, the cytoplasmic β subunit (IFN-γR2) of interferon-γ receptor (IFN-γR) is induced and translocates to plasma membrane to join α subunit to form functional IFN-γR to mediate IFN-γ signaling. However, the mechanism driving membrane translocation and its significance remain largely unknown. We found, unexpectedly, that mice deficient in E-selectin, an endothelial cell-specific adhesion molecule, displayed impaired innate activation of macrophages upon *Listeria monocytogenes* infection yet had increased circulating IFN-γ. Inflammatory macrophages from E-selectin-deficient mice had less surface IFN-γR2 and impaired IFN-γ signaling. BTK elicited by extrinsic E-selectin engagement phosphorylates cytoplasmic IFN-γR2, facilitating EFhd2 binding and promoting IFN-γR2 trafficking from Golgi to cell membrane. Our findings demonstrate that membrane translocation of cytoplasmic IFN-γR2 is required to activate macrophage innate response against intracellular bacterial infection, identifying the assembly of functional cytokine receptors on cell membrane as an important layer in innate activation and cytokine signaling.

INTRODUCTION

Interferon-gamma (IFN-γ) plays crucial roles in immunity and inflammation. Upon engagement of the IFN-γ receptor (IFN-γR), IFN-γ triggers intracellular signals through the Janus kinase (JAK)-signal transducer and activator of transcription (STAT) pathway to achieve transcriptional control of IFN-γ-inducible genes (Schoenborn and Wilson, 2007). Proper activation of IFN-γ signaling orchestrates diverse cellular programs including promoting macrophage activation, mediating host defense against intracellular bacterial infection. Correspondingly, the dysregulation of IFN-γ signaling has been linked to pathogenesis of various inflammatory and immunological disorders (Hu and Ivashkiv, 2009). IFN-γ also plays an immunoregulatory role in anti-tumor immunity and has been proposed to regulate responsiveness to immune checkpoint blockade (Benci et al., 2016). Complex molecular mechanisms have evolved to control the immune response triggered by IFN-γ to ensure protective immune responses and avoid unwanted immunopathology. These controls work at many different levels, from transcriptional and post-transcriptional regulation of IFN-γ expression (Gomez et al., 2013), to regulation of JAK/STAT signaling mediated by IFN-γ engagement with functional IFN-γR on cell membrane (Ma et al., 2011). However, the mechanisms governing membrane presentation and functional assembly of IFN-γR remain elusive.

Functional IFN-γR is composed of two subunits: IFN-γ receptor α (IFN-γR1) and IFN-γ receptor β (IFN-γR2). IFN-γR1, constitutively expressed on all nucleated cells, is responsible for binding IFN-γ, IFN-γR2 is induced after bacterial infection and then translocates to cell membrane where it forms functional IFN-γR (Bach et al., 1997; Blouin and Lamaze, 2013). The intensity of cell membrane level of receptors is decided by a series of dynamic processes including delivery of *de novo* synthesis, endocytosis, recycling, and degradation. IFN-γR2 is differentially expressed among the immune cells, high in B and myeloid cells but low or absent in T cells (Bernabei et al., 2001). Downregulation of IFN-γR2 in Th1 cell is a negative mechanism to limit the apoptotic effect of IFN-γ (Bach et al., 1995). High expression of IFN-γR2 on macrophages favors IFN-γ-mediated apoptosis of mycobacteria-infected macrophages (Oddo et al., 1998). Many studies investigated the mechanisms of IFN-γR2 internalization in T cells. Ligand-dependent or independent internalization of IFN-γR2 was founded in T cells (Pernis et al., 1995; Groux et al., 1997). IGF-1 was previously shown to mediate IFN-γR2 internalization in T lymphocytes, but not in B cells or myeloid cells (Bernabei et al., 2003). IFN-γ does not affect IFN-γR2 expression on macrophages (Hu et al., 2002). Glycosylation of

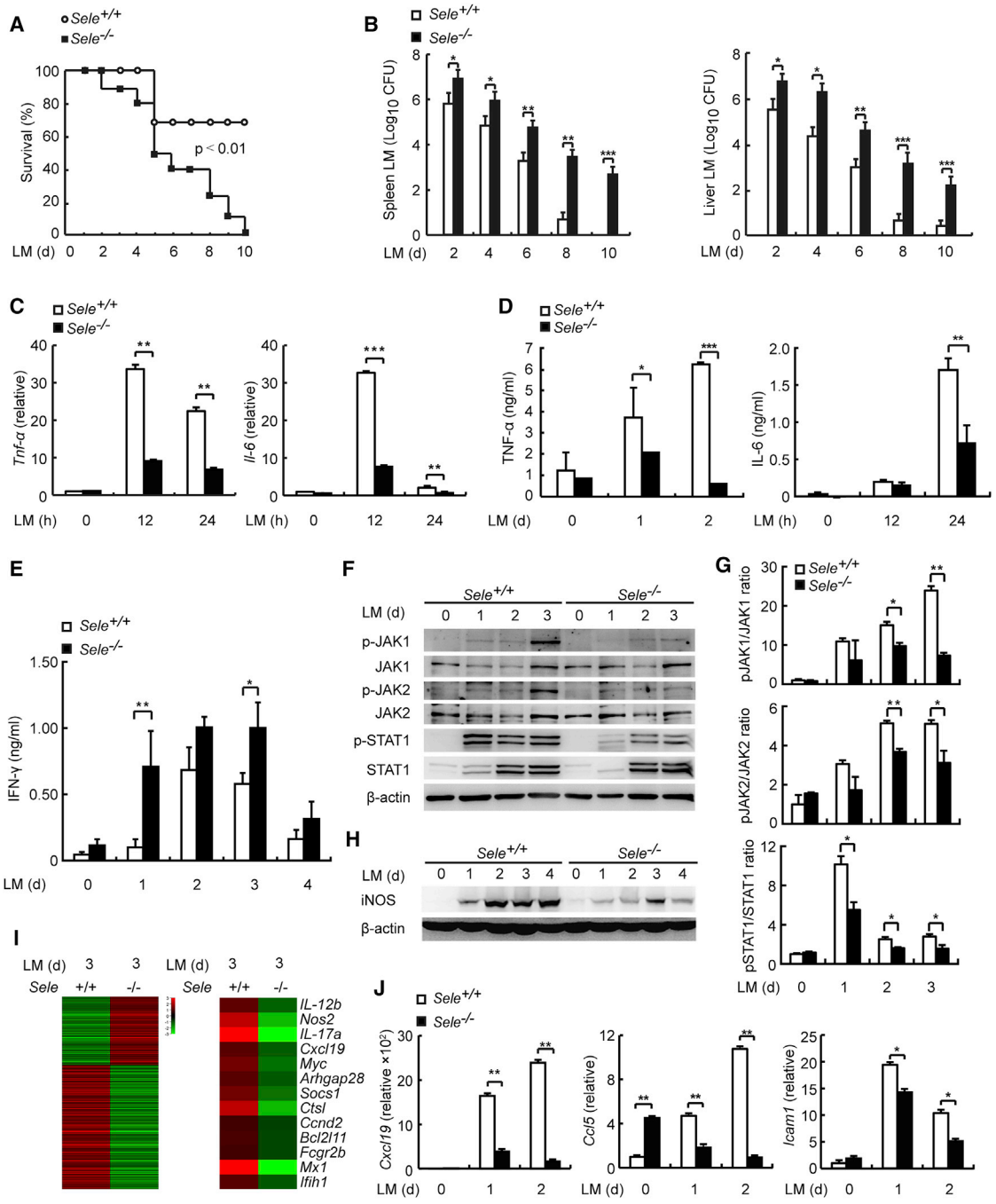

Figure 1. *Sele*$^{-/-}$ Mice Exhibit Increased Susceptibility to LM Infection and Reduced Macrophage Activation

(A–H) *Sele*$^{-/-}$ and *Sele*$^{+/+}$ mice were challenged with LM for indicated days and subjected to the following assays.

(A) Survival of *Sele*$^{-/-}$ and *Sele*$^{+/+}$ mice infected with LM (n = 10 per genotype) was monitored every day (Wilcoxon test).

(B) Colony-forming units (CFUs) were assayed in spleens and livers (n = 5 per genotype).

(C) *Tnf-α* and *Il-6* mRNA in PMs were determined by qRT-PCR.

(D) TNF-α and IL-6 in sera was determined by ELISA (n = 3 per group).

(E) IFN-γ in sera was determined by ELISA.

(F and G) Phosphorylated (p) signaling molecules of IFN-γ in PMs lysates were measured by immunoblot (IB) analysis (F) and quantification analysis (G).

(H) iNOS in PMs lysates was examined by IB analysis.

(I) Microarray analysis of *Sele*$^{-/-}$ and *Sele*$^{+/+}$ PMs were analyzed. The left heatmap shown differentially expressed genes, the differentially expressed ISGs are shown on the right.

(legend continued on next page)

IFN-γR2 is involved in IFN-γ signaling via affecting dynamic receptor interactions with actin and lipid nanodomains (Blouin et al., 2016)· Notably, abnormalities in IFN-γR1 and IFN-γR2 expression are closely associated with Mendelian susceptibility to mycobacterial disease (MSMD), a syndrome characterized by localized or disseminated infections caused by atypical mycobacteria (Sharma et al., 2015). Given the critical roles of IFN-γR2 in immunity and disease, understanding the mechanisms controlling translocation of IFN-γR2 from cytosol to membrane in immune cells such as macrophages has important biological significance and clinical implications.

E-selectin (endothelial selectin) is inducible on vascular endothelial cells during inflammation, and it engages counter-ligands on leukocytes to induce leukocyte movement via signaling pathways, such as bruton tyrosine kinase (BTK), in many physiological and pathological processes (Mueller et al., 2010; Winkler et al., 2012). In an attempt to clarify the role of E-selectin-dependent innate immune cell migration, we studied the innate activation of macrophages in E-selectin-deficient mice upon infection with *Listeria monocytogenes* (LM). Surprisingly we observed highly elevated levels of IFN-γ in blood but significantly attenuated IFN-γ signaling and impaired innate function of macrophages from E-selectin-deficient mice. This unexpected finding of higher IFN-γ levels but impaired IFN-γ signaling promoted us to investigate the underlying mechanism, and we found that E-selectin engagement is required for membrane translocation of IFN-γR2 from Golgi and assembly of functional IFN-γR on macrophages. E-selectin engagement provides the signal to activate the BTK kinase, which phosphorylates tyrosine 289 of IFN-γR2 in the cytoplasm. Subsequently, EFhd2 binds phosphorylated IFN-γR2Y289 to promote its membrane translocation, ultimately leading to functional IFN-γR formation and enabling IFN-γ binding to functional IFN-γR and triggering efficient innate response of macrophages against intracellular bacterial infection. Our results establish a paradigm for the signaling elicited in macrophages by extrinsic E-selectin engagement that promotes formation of functional cytokine receptors. Furthermore, the crosstalk between immune cell migration from vessels and cytokine signaling in innate response adds new insight to the biology of cytokine signaling.

RESULTS

Deficiency of E-Selectin Attenuates Innate Defense against LM Infection but Increases Circulating IFN-γ Levels

To clarify the role of E-selectin in innate activation during the host immune response to pathogenic infection, we first examined the susceptibility of mice lacking the *Sele* gene (encoding E-selectin) (*Sele*$^{-/-}$) and their littermates, *Sele*$^{+/+}$ mice, to LM infection *in vivo*. Immunohistochemistry analysis showed inducible expression of E-selectin in the spleen of wild-type mice after LM infection (Figure S1A). The *Sele*$^{-/-}$ mice were more sensitive to LM infection in overall survival assays (Figure 1A). The decreased survival rate of *Sele*$^{-/-}$ mice after LM infection was consistent with the marked increased in LM abundance in the spleen and liver (Figure 1B) and the smaller size of the spleen (Figure S1B), which confirmed the increased susceptibility to LM infection in the absence of E-selectin.

Monocytes/macrophages are major contributors to innate defense against LM infection, we therefore analyzed whether alterations of macrophage function and/or activation were involved in the increased susceptibility of *Sele*$^{-/-}$ mice to LM infection. Both mRNA and protein levels of *Tnf-α* and *Il-6* were significantly decreased in *Sele*$^{-/-}$ mice (Figures 1C and 1D), indicating decreased macrophage activation in *Sele*$^{-/-}$ mice upon LM infection.

IFN-γ signaling is essential to macrophage activation for clearance of intracellular bacterium such as LM (Pamer, 2004). Unexpectedly, we found there were significantly increased levels of IFN-γ in the serum of *Sele*$^{-/-}$ mice (Figure 1E). However, phosphorylation of JAK1/2 and STAT1 (Figures 1F and 1G), as well as the expression of iNOS protein (Figure 1H) were decreased in peritoneal macrophages (PMs) from *Sele*$^{-/-}$ mice infected with LM. Moreover, microarray analysis showed a series of IFN-stimulated genes (ISGs) of IFN-γ signaling, such as *Cxcl19*, *Nos2*, and *Fcgr2b*, were downregulated in macrophages from LM-infected *Sele*$^{-/-}$ mice (Figure 1I). qRT-PCR confirmed the decreased expression of several ISGs including *Cxcl19*, *Ccl5*, and *Icam1* in PMs from *Sele*$^{-/-}$ mice (Figure 1J). To determine the cellular source of elevated IFN-γ production in *Sele*$^{-/-}$ mice, we analyzed the expression of intracellular IFN-γ in CD4^{+} T cells, CD8^{+} T cells, and natural killer (NK) cells from LM-infected mice. IFN-γ production in these cells was comparable between *Sele*$^{+/+}$ and *Sele*$^{-/-}$ mice infected with LM (Figures S1C–S1E).

Taken together, we showed that *Sele*$^{-/-}$ mice displayed increased susceptibility to LM infection, which is accompanied by impaired IFN-γ signaling and decreased production of innate cytokines in macrophages, but unexpectedly exhibited higher IFN-γ in the blood.

Deficiency of E-Selectin Decreases Surface Levels of IFN-γR2 on Macrophages

E-selectin was previously shown to regulate hematopoietic stem cell dormancy and self-renewal (Winkler et al., 2012). We found the percentages of immune cells including B cells, CD4^{+} T cells, CD8^{+} T cells, dendritic cells, and macrophages were intact in *Sele*$^{-/-}$ spleens, whereas the ratio of splenic NK cells was much lower in *Sele*$^{-/-}$ mice compared with *Sele*$^{+/+}$ mice without LM infection (Figure S2A). Thus, deletion of E-selectin affected the development of NK cells, excluding the possibility that NK cells are the cellular source for the higher IFN-γ in the blood of *Sele*$^{-/-}$ mice upon LM infection.

IFN-γR1 is constitutively expressed and binds to IFN-γ, while IFN-γR2, which controls signaling, is induced upon stimulation

(J) ISGs mRNA in PMs was determined by qRT-PCR.

Data are shown mean ± SD of three independent experiments (A–E, G, I, and K) or one representative of three independent experiments with similar results. *p < 0.05, **p < 0.01, ***p < 0.01, (Student's t test).

See also Figure S1.

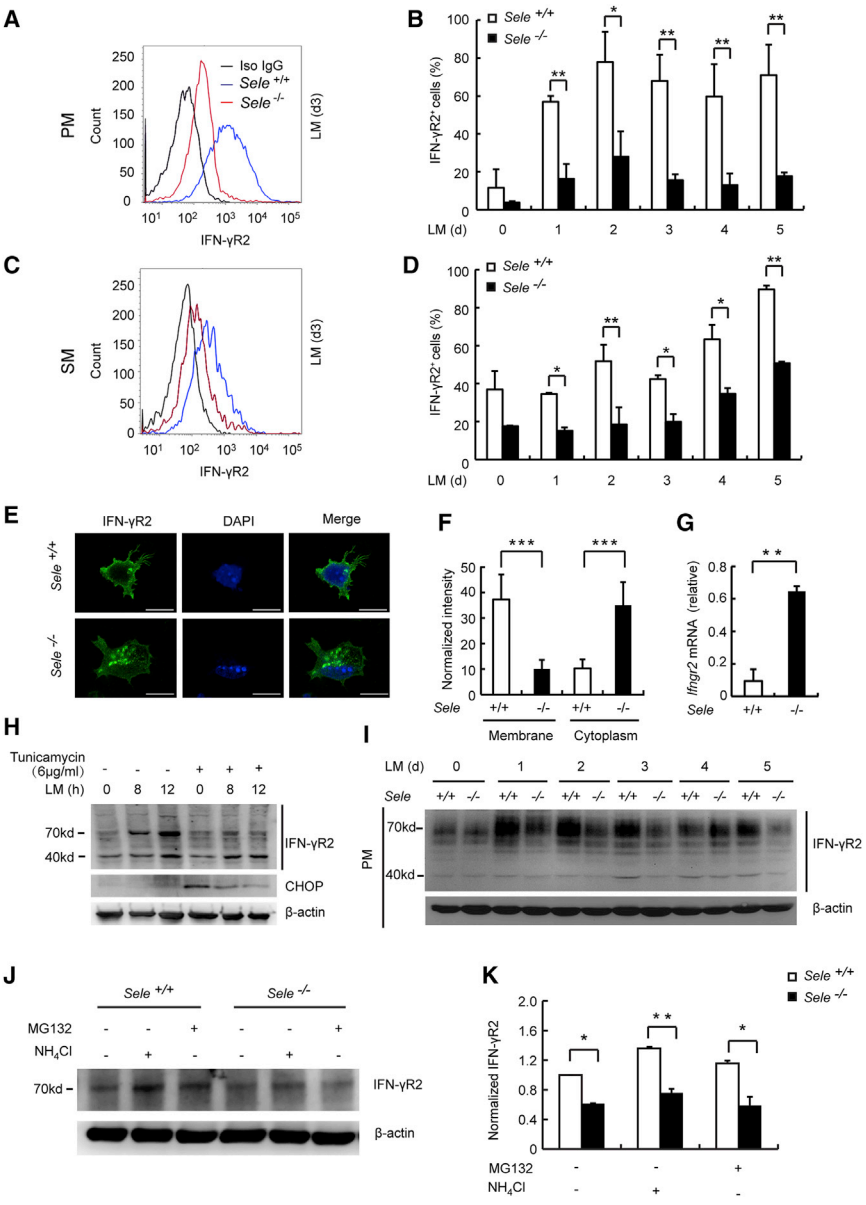

Figure 2. Decreased Membrane Localization but Unchanged Protein Levels of IFN-γR2 in Macrophages from LM-Infected *Sele*$^{-/-}$ Mice

(A–F) *Sele*$^{-/-}$ and *Sele*$^{+/+}$ mice were challenged without or with LM and subjected to the following assays, (n = 5 per group). (A–D) IFN-γR2 membrane expression of PMs (A and B) or SM (C and D) was determined by flow cytometry. (E and F) Representative images of immunofluorescence (E), and quantification of IFN-γR2 intensity on membrane or in cytoplasm of PMs (50 cells in each group) was normalized by area (F). Scale bar, 10 μm.

(G) *Ifngr2* mRNA in PMs was determined by qRT-PCR.

(H) IB analysis of glycosylated IFN-γR2 in BMDMs pretreated with inhibitor of N-linked glycosylation in response of LM stimulation *in vitro*, with CHOP as positive control.

(I) IFN-γR2 in PMs lysates was detected by IB analysis.

(J) Immunoblot analysis of IFNγR2 in lysates of *Sele*$^{-/-}$ and *Sele*$^{+/+}$ PMs treated with NH_4Cl (10 mM) or MG132 (10 μM) for 6 hr before harvest.

(K) Quantification of band intensity of IFNγR2 in the blot of (J), normalized to the value for cells without treatment.

Data are shown mean ± SD of three independent experiments (right panels of A, B, and K) or one representative of three independent experiments with similar results. *$p < 0.05$, **$p < 0.01$, (Student's t test).

See also Figure S2.

(Stark and Darnell, 2012). We hypothesized that in the absence of E-selectin, there is abnormal membrane expression of IFN-γR2 on immune cells, leading to impaired activation of macrophages in response to LM infection. Notably, flow cytometry analysis showed markedly decreased levels of membrane IFN-γR2 in both peritoneal and splenic macrophages (SMs) of *Sele*$^{-/-}$ mice compared with control after LM infection (Figures 2A–2D). Immunofluorescence analysis also confirmed the decreased IFN-γR2 on the membrane and increased IFN-γR2 in the cytoplasm of PMs in LM-infected *Sele*$^{-/-}$ mice (Figures 2E and 2F). The membrane IFN-γR2 were also decreased on NK cells and dendritic cells in LM-infected *Sele*$^{-/-}$ mice, but there was no difference on CD4$^+$ T cells, CD8$^+$ cells, or B cells (Figure S2B). Our fluorescence-activated cell sorting (FACS) analysis showed that E-selectin had no significant effect on IFN-γR1 membrane expression in PMs (Figure S2C).

To confirm the specificity of IFN-γR2 antibody used in this study, we generated *Ifngr2* knockout RAW264.7 cells by CRISPR/Cas9, and our western blot showed that four bands including 40 kDa, 50 kDa, 65 kDa, and 70 kDa were deleted in the *Ifngr2* knockout RAW264.7 cells, which suggests these bands are IFN-γR2 in different modifications (Figure S2D). We then confirmed the specificity of anti-IFN-γR2 antibody used in this study for FACS analysis by examination of IFN-γR2 membrane expression in *Ifngr2* WT and KO RAW264.7 cells (Figure S2E). Two clones of *Ifngr2* KO RAW264.7 cells showed completely inhibited phosphorylation of JAK/STAT molecules upon IFN-γ stimulation (Figure S2F), suggesting the phosphorylation of the molecules of JAK/STAT signaling is specifically triggered by IFN-γ binding with IFN-γR.

Interestingly, we found that the mRNA level of *Ifngr2* was increased in PMs of LM-infected *Sele*$^{-/-}$ mice (Figure 2G). Membrane proteins are subjected to various post-translational processing and modification, such as glycosylation, which are functionally important. We performed western blotting to identify

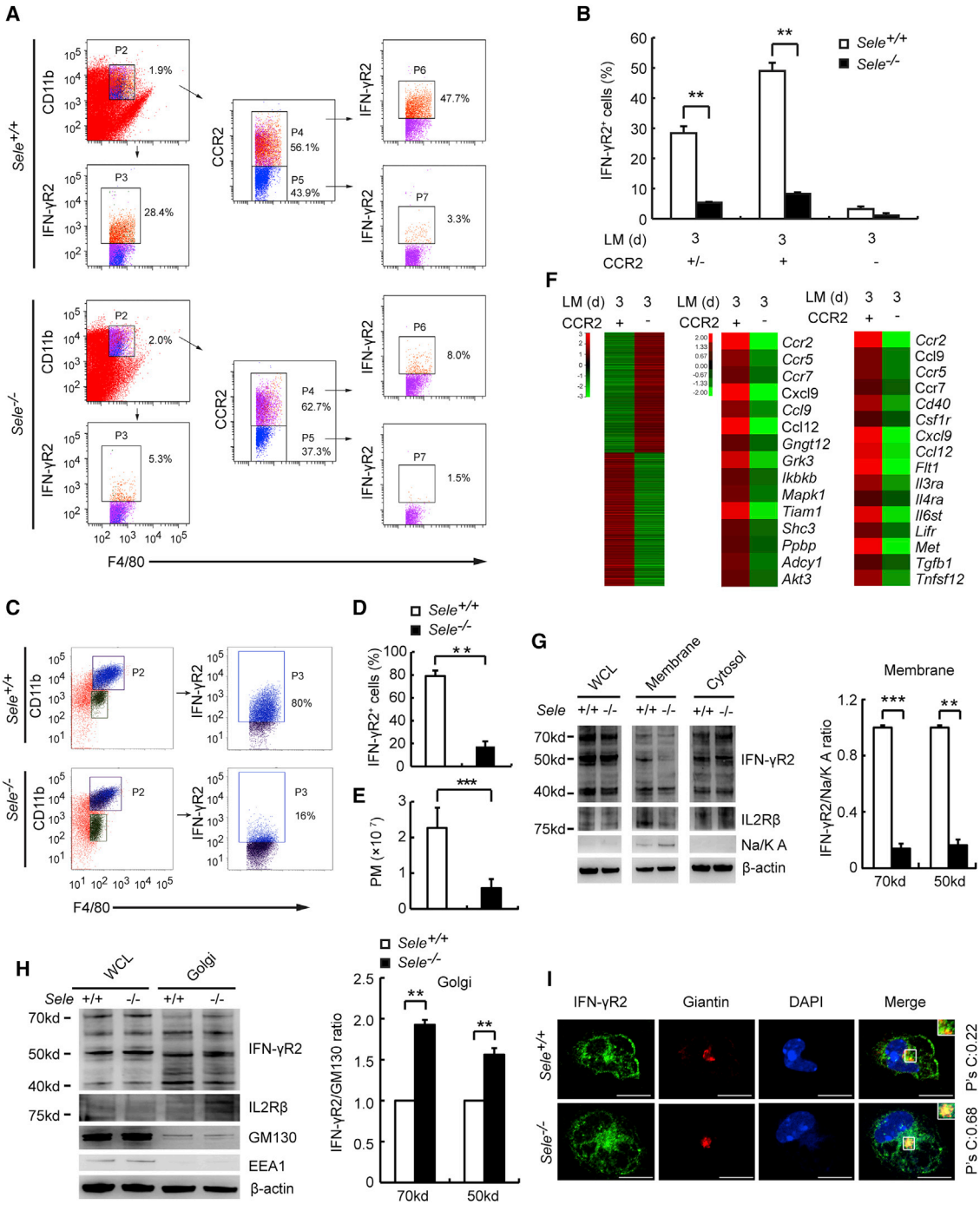

Figure 3. Decreased IFN-γR2 Membrane Localization on Inflammatory Macrophages in LM-Infected *Sele*$^{-/-}$ Mice

(A) Flow cytometry analysis of membrane IFN-γR2 on CCR2^{+} or CCR2^{-} SMs of *Sele*$^{+/+}$ or *Sele*$^{-/-}$ mice infected with LM for 3 days (n = 5 per group).

(B) Quantitative analysis of the percentages of IFN-γR2 expression on the membrane of total SMs, CCR2^{+}and CCR2^{-} SMs from (A), (n = 5 per group).

(C and D) Flow cytometry (C) and quantitative analysis (D) of the percentage of surface IFN-γR2^{+} on CD11b^{+}/F4/80^{+} macrophages (P2) recruited by thioglycolate broth intraperitoneal injection from *Sele*$^{+/+}$ or *Sele*$^{-/-}$ mice (n = 5 per group).

(E) The number of macrophages migrated to the peritoneal cavity from *Sele*$^{+/+}$ and *Sele*$^{-/-}$ mice on day 3 after thioglycolate broth injection (n = 5 per group).

(F) Microarray analysis of CCR2^{+} and CCR2^{-} SMs from the mice infected with LM *in vivo*. Left heatmap: all the differential genes. Middle heatmap: genes involved in chemokine pathway upregulated in CCR2^{+} macrophages. Right heatmap: genes involved in cytokine-cytokine receptor interactions upregulated in CCR2^{+} macrophages.

(legend continued on next page)

the molecular size of glycosylated IFN-γR2 in the lysis of BMDMs pretreated without or with N-glycosylation inhibitor tunicamycin. Our results showed one 70 kDa band was significantly decreased after treatment with tunicamycin (Figure 2H), which indicates that this band is N-glycosylated IFN-γR2. We further confirmed that non-modified IFN-γR2 was comparable between *Sele*$^{-/-}$ and *Sele*$^{+/+}$ PMs, suggesting the synthesis of IFN-γR2 was not affected by E-selectin. Decreased levels of glycosylated IFN-γR2 were found in PMs of LM-infected *Sele*$^{-/-}$ mice relative to levels in wild-type mice (Figure 2I). We also found that the expression of modified IFNγR2 (70 kDa) in *Sele*$^{-/-}$ PMs treated with inhibitors NH_4Cl or MG132 was not rescued compared with control (Figures 2J and 2K). In conclusion, E-selectin is required for the membrane location of IFN-γR2 in macrophages during LM infection.

Deficiency of E-Selectin Decreases Membrane Translocation of IFN-γR2 from Golgi on CCR2$^+$ Inflammatory Macrophages

We next asked whether other membrane receptors on macrophages were similarly regulated by E-selectin. Membrane levels of subunit β of the IL-2 receptor (IL-2Rβ) that is constitutively expressed and inducible receptor for IL-2 (Malek and Castro, 2010), as well as TLR4 (Brubaker et al., 2015), were significantly decreased on splenic and peritoneal macrophages in LM-infected *Sele*$^{-/-}$ mice (Figures S3A–S3C). These results suggest broad significance of E-selectin signaling in driving membrane expression of innate receptors.

Macrophages can be broadly categorized into two subsets according to their location at either inflammatory or resident lesions: CCR2$^+$ macrophages are known as "migratory" or "inflammatory" macrophages, and CCR2$^-$ macrophages are known as "resident" macrophages (Udalova et al., 2016). CCR2$^+$ macrophages displayed significantly higher membrane IFN-γR2 levels than CCR2$^-$ macrophages. Moreover, CCR2$^+$ macrophages in LM-infected *Sele*$^{-/-}$ mice displayed much less membrane IFN-γR2 than in LM-infected *Sele*$^{+/+}$ mice (Figures 3A and 3B). Similarly, after intraperitoneal (i.p.) infection of thioglycolate broth, *Sele*$^{-/-}$ mice had significantly decreased membrane IFN-γR2 on CD11b$^+$/F4/80$^+$ PMs (Figures 3C and 3D) and decreased number of recruited PMs (Figure 3E) relative to *Sele*$^{+/+}$ mice. This suggests membrane expression of IFN-γR2 is differentially regulated in resident and inflammatory macrophages and impaired only in inflammatory macrophages in *Sele*$^{-/-}$ mice.

To clarify the characteristics of CCR2$^-$ and CCR2$^+$ macrophages, we sorted and analyzed the differential genes between CCR2$^-$ and CCR2$^+$ SMs upon LM infection by microarray. A series of genes involved in cell chemotaxis as well as a set of genes involved in cytokine-cytokine receptor interactions were significantly upregulated in CCR2$^+$ macrophages compared with CCR2$^-$ macrophages (Figure 3F). This indicates that CCR2$^+$ inflammatory macrophages recruited from vessels into inflamed tissue play critical functions in defense of intracellular bacterial infection, which might be carried out by inducible membrane expression of IFN-γR2 on this subset of macrophages.

The number of receptors on the membrane is regulated by a series of dynamic processes including delivery of *de novo* synthesis, endocytosis, recycling, and degradation. We set out to identify which part of the processes was impaired in *Sele*$^{-/-}$ macrophages. We isolated membrane, cytosol, endosome, and Golgi of *Sele*$^{+/+}$ and *Sele*$^{-/-}$ PMs and performed western blotting to examine the level of IFN-γR2 protein in these cell fractions. The protein in the cytosol was comparable between *Sele*$^{-/-}$ and *Sele*$^{+/+}$ PMs. However, IFN-γR2 protein was significantly decreased in the cell membrane (Figure 3G) and endosome (Figure S3D) of *Sele*$^{-/-}$ PMs compared with control. On the contrary, IFN-γR2 level was significantly increased in Golgi isolated from *Sele*$^{-/-}$ PMs compared with control (Figure 3H). Immunofluorescence analysis further confirmed that endogenous IFN-γR2 accumulated in Golgi of PMs after deletion of *Sele* (Figure 3I). We also confirmed the IL2Rβ protein was decreased in the isolated cell membrane (Figure 3G) and endosome (Figure S3D) but increased in Golgi of *Sele*$^{-/-}$ PMs (Figure 3H).

Rab family is involved in endocytosis (Rab5), recycling (Rab11), and degradation (Rab7) of receptors (Stenmark, 2009). To further clarify whether or not E-selectin has effect on endocytosis, recycling, and degradation of IFN-γR2, we performed immunofluorescence to examine the colocalization between IFN-γR2 and Rab5, Rab11, or Rab7 in *Sele*$^{-/-}$ and *Sele*$^{+/+}$ PMs from the mice after infection with LM 3 days. The decreased colocalization between IFN-γR2 and Rab5 was observed in *Sele*$^{-/-}$ PMs (Figure S3E), which indicated decreased IFN-γR2 on membrane was not caused by enhanced endocytosis. In addition, decreased colocalization between IFN-γR2 and Rab7 in *Sele*$^{-/-}$ PMs (Figure S3G) ruled out the possibility of increased degradation in lysosome leading to decreased IFN-γR2 on membrane. Our data of decreased colocalization between IFN-γR2 and Rab11 (Figure S3F) suggested that recycling of IFN-γR2 was also declined in *Sele*$^{-/-}$ PMs, and we speculated that decreased recycling in *Sele*$^{-/-}$ PMs might be caused by the decreased endocytosis. We then immediately labeled the freshly isolated primary PMs with biotin to confirm whether E-selectin affected endocytosis and recycling of IFN-γR2. We found that the ratio of endocytosis (internalized/surface) and recycling (internalized/recycled) of IFNγR2 was comparable between *Sele*$^{-/-}$ and *Sele*$^{+/+}$ PMs (Figures S3H–S3J), confirming that E-selectin didn't regulate membrane expression of IFNγR2 by affecting its endocytosis and recycling.

(G and H) IB analysis of IFN-γR2 or IL2Rβ and quantifications of IFN-γR2 in the isolated membrane (G; All samples were run on the same gel) and Golgi (H) from *Sele*$^{+/+}$ and *Sele*$^{-/-}$ PMs.

(I) Staining of IFN-γR2 and giantin in *Sele*$^{+/+}$ and *Sele*$^{-/-}$ PMs infected with LM for 3 days (scale bar, 10 μm). Na/K A: Na/K ATPase. P's C: Pearson's correlation coefficient.

Data are shown mean ± SD of three independent experiments (B–D) or one representative of three independent experiments with similar results. **$p < 0.01$, ***$p < 0.001$ (Student's t test).

See also Figure S3.

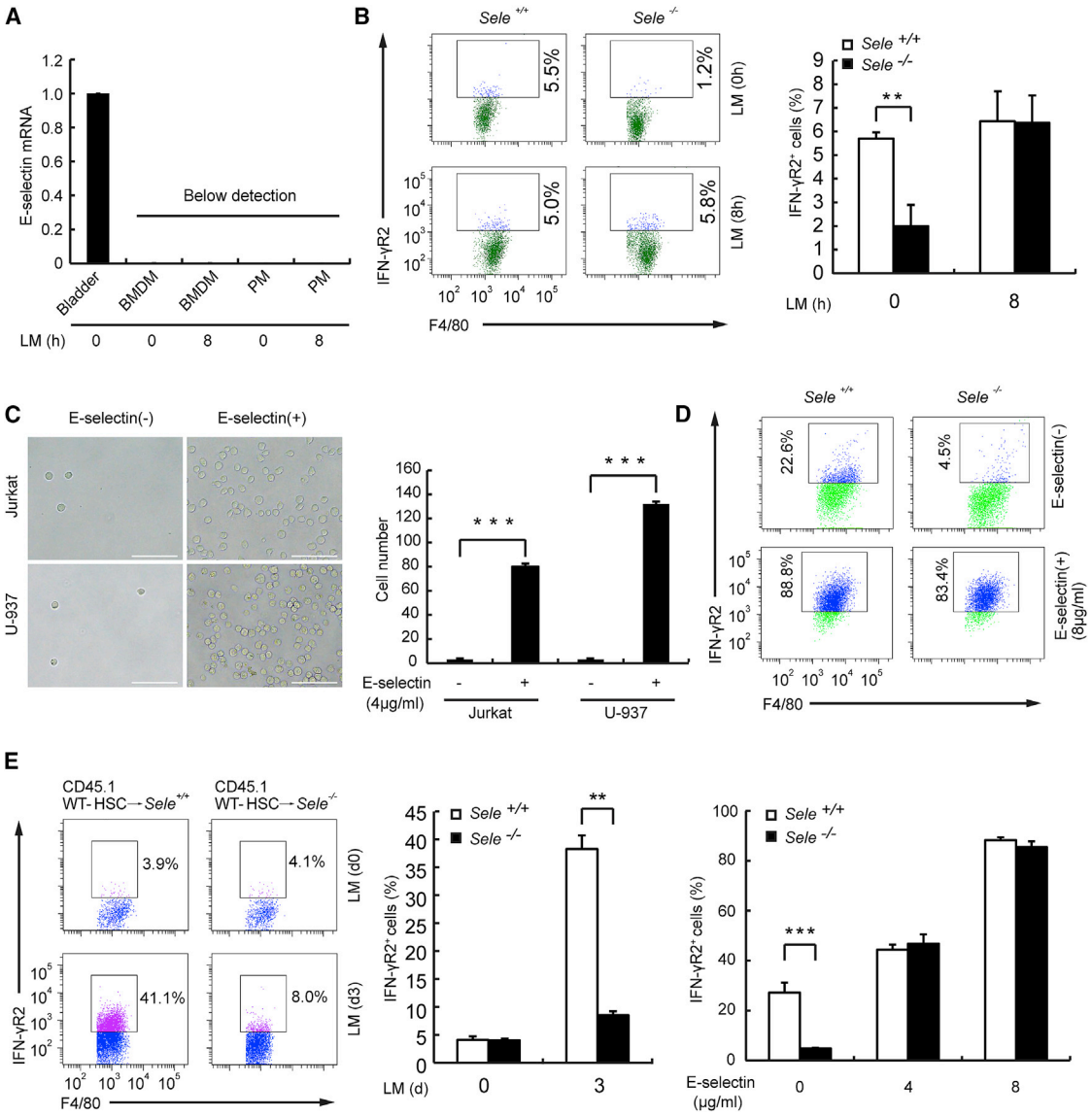

Figure 4. Vascular E-Selectin Is Crucial for Membrane Translocation of IFN-γR2 in Macrophages

(A) *Sele* mRNA in BMDMs and PMs was examined by qRT-PCR, with bladder tissue as positive control.

(B) Representative FACS and quantification of membrane IFN-γR2$^+$ macrophages sorted from bone marrow stimulated without or with LM for 2 hr (n = 5 per group).

(C) Representative images and quantification of attached cells Jurkat and U-937 on the plate coated with recombinant E-selectin (4 μg/mL; scale bar, 100 μm).

(D) *Sele*$^{+/+}$ or *Sele*$^{-/-}$ PMs were incubated in the dishes coated with recombinant E-selectin (4 μg/mL or 8 μg/mL) 8 hr, and FACS analysis and quantification of membrane IFN-γR2$^+$ cells were performed (n = 3 per group).

(E) Membrane IFN-γR2$^+$ PMs from HSC transplanted mice infected without or with LM on day 3 were determined by FACS. Quantitative analysis of the percentage of membrane IFN-γR2$^+$ macrophages is shown in the right panel.

Data are shown mean ± SD, (n = 5 per group). Data are shown mean ± SD of three independent experiments (A–E) or one representative of three independent experiments with similar results. **p < 0.01, ***p < 0.001 (Student's t test).

See also Figure S4.

In addition, our results (Figures 2I–2K) showed that synthesis and degradation processes were not involved in the regulation of membrane expression of IFN-γR2 by E-selectin. Therefore, we speculated that the increased level of IFN-γR2 protein in Golgi after deletion of *Sele* gene led to its impaired transport to membrane.

E-Selectin Engagement Promotes Membrane Translocation of IFN-γR2 in Macrophages

E-selectin is specifically expressed on the inflamed endothelial cells (Zarbock et al., 2008). Is E-selectin expressed or inducible in macrophages in response to LM stimulation? Moreover, is the function of E-selectin in regulation of IFN-γR2 membrane

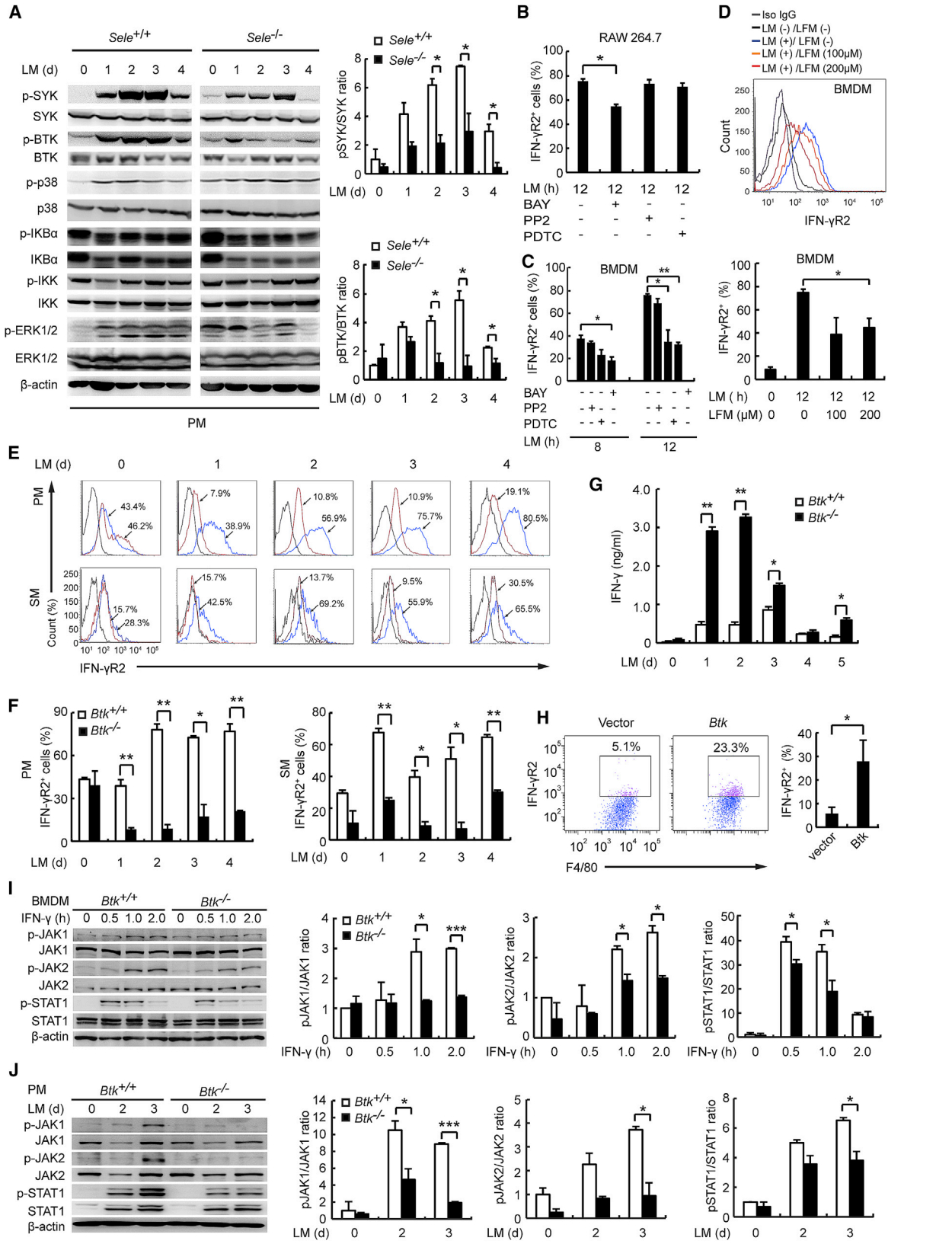

(legend on next page)

expression on macrophages cell intrinsic or cell extrinsic? Mouse ENCODE transcriptome data show that *Sele* mRNA is only highly expressed in bladder and placenta of adult mouse, we then examined expression of *Sele* mRNA in the BMDMs and PMs of *Sele*$^{+/+}$ mice controlled with bladder tissue. Our results showed that *Sele* mRNA was undetectable and was not inducible in BMDMs or PMs in response to LM stimulation (Figure 4A). Our FACS analysis showed that there was comparable membrane expression of IFN-γR2 between sorted *Sele*$^{+/+}$ and *Sele*$^{-/-}$ macrophages from bone marrow stimulated with LM (Figure 4B). These results indicated that E-selectin regulated the macrophage membrane expression of IFN-γR2 in manner of cell extrinsic.

We also analyzed the contribution of purified recombinant E-selectin to the membrane localization of IFN-γR2. We detected the adhesion activity of recombinant E-selectin by attachment of Jurkat and U-937 cells with the coated protein on the dish (Figure 4C). Our FACS analysis showed that recombinant E-selectin could rescue the membrane expression of IFN-γR2 on *Sele*$^{-/-}$ macrophages dose dependently (Figure 4D), further confirming the E-selectin functions in regulating IFN-γR2 membrane expression on macrophages.

To exclude the possibility of contamination of bone marrow endothelial cells, we sorted bone marrow hematopoietic stem cells (HSCs) and performed HSC transplantation to determine whether E-selectin on endothelial cells was responsible for driving IFN-γR2 membrane translocation *in vivo*. We transplanted CD45.1^{+} *Sele*$^{+/+}$ HSCs sorted from bone marrow of CD45.1^{+} C57BL/6 mice to *Sele*$^{+/+}$ or *Sele*$^{-/-}$ mice. In response to LM infection, the *Sele*$^{-/-}$ recipients receiving *Sele*$^{+/+}$ HSCs had significantly decreased membrane expression of IFN-γR2 on PMs as compared with *Sele*$^{+/+}$ recipients receiving *Sele*$^{+/+}$ HSC. This demonstrates that host E-selectin on endothelial cells is responsible for promoting IFN-γR2 membrane translocation *in vivo* (Figure 4E).

Several ligands for E-selectin on leukocytes have been identified, such as P-selectin glycoprotein ligand-1 (PSGL-1) (Xia et al., 2002) and (macrophage antigen-1) Mac-1 (Crutchfield et al., 2000). We examined the membrane levels of IFN-γR2 on PMs from PSGL-1$^{-/-}$ or Mac-1$^{-/-}$ mice infected with LM. However, deletion of either *Psgl-1*$^{-/-}$ or *Mac-1*$^{-/-}$ had no effect on IFN-γR2 membrane levels (Figures S4A and S4B). Future work is needed to identify the precise ligands on macrophages responsible for E-selectin engagement in this process.

E-Selectin Engagement-Activated BTK Contributes to Membrane Translocation of IFN-γR2

Phosphokinase spleen tyrosine kinase (SYK) and bruton tyrosine kinase (BTK) are important in the signaling pathways triggered by engagement of E-selectin on endothelial cells with its ligands on leukocytes (Zarbock et al., 2008; Mueller et al., 2010). We therefore examined the status of specific signaling molecules including SYK, BTK, and the nuclear factor κB (NF-κB) and mitogen-activated protein kinase (MAPK) pathways in PMs from LM-infected *Sele*$^{-/-}$ or *Sele*$^{+/+}$ mice. The phosphorylation of both SYK and BTK was significantly reduced in macrophages from *Sele*$^{-/-}$ mice, with no obvious changes in other phosphorylated proteins (Figure 5A). To further analyze whether SYK and BTK participated in IFN-γR2 translocation, we pretreated the macrophage cells RAW264.7 and BMDMs with a specific inhibitor for SYK, BAY61-3606, and found reduced levels of membrane IFN-γR2 on LM-stimulated RAW264.7 cells (Figure 5B) and BMDMs (Figure 5C). The specific inhibitor for NF-κB, PDTC, also inhibited IFN-γR2 translocation in BMDMs, while PP2, the inhibitor for Src, had no such effect (Figure 5C). Therefore, SYK may be involved in driving cytoplasmic IFN-γR2 to the membrane in macrophages. BTK is the downstream molecule of SYK in E-selectin signaling. Accordingly, the specific BTK inhibitor LFM-A13 significantly reduced membrane expression of IFN-γR2 (Figure 5D). We further confirmed the decreased activation of JAK/STAT signaling in the BMDMs of C57BL/6 mice pretreated with the inhibitors or silenced expression of the genes *Syk*, *Btk*, and *P65* in response to IFN-γ stimulation (Figures S5A–S5F). The results indicated that these molecules were involved in regulation of IFN-γR2 membrane expression on macrophages.

Similar to *Sele*$^{-/-}$ mice, *Btk*$^{-/-}$ mice, upon LM infection, also showed significantly decreased membrane expression of IFN-γR2 on macrophages (Figures 5E and 5F) as well as elevated levels of serum IFN-γ as compared to their littermate *Btk*$^{+/+}$ mice (Figure 5G). While exogenous expression of BTK rescued the membrane expression of IFN-γR2 in macrophages from *Sele*$^{-/-}$ mice (Figure 5H). The activation of JAK/STAT pathway

Figure 5. E-Selectin Engagement-Activated Phosphokinases SYK and BTK Promote IFN-γR2 Membrane Translocation

(A) IB analysis and quantification of phosphorylated (-p) proteins in PMs lysates of *Sele*$^{+/+}$ and *Sele*$^{-/-}$ mice infected with LM for indicated times.

(B) RAW264.7 cells were pre-treated with inhibitors BAY61-3606 (BAY), PP2, or PDTC for 1 hr and then stimulated with LM for 12 hr. Membrane IFN-γR2^{+} cells were analyzed by FACS.

(C) BMDMs were pre-treated, stimulated, and then assessed as in (B).

(D) BMDMs were pre-treated with a specific inhibitor for BTK, LFM-A13 (LFM), for 1 hr, stimulated with LM for 12 hr, and then assessed by FACS for IFN-γR2 expression (top). Quantification analysis (bottom).

(E–G) *Btk*$^{-/-}$ and *Btk*$^{+/+}$ mice were challenged with LM for the indicated days and subjected to the following assays. (E) FACS analysis of membrane IFN-γR2 expression on PMs and SMs. The black, blue, and red lines represented isotype IgG, *Btk*$^{-/-}$ macrophages, and *Btk*$^{+/+}$ macrophages, respectively. (F) Quantification of membrane IFN-γR2^{+} cells from E. (G) ELISA of IFN-γ concentration in sera.

(H) *Sele*$^{-/-}$ BMDMs were transfected with plasmid encoding BTK and stimulated with LM and then IFN-γR2 membrane expression was examined by FACS, with vector transfection as negative control.

(I and J) IB analysis of JAK/STAT molecules in the lysates of BMDMs stimulated with IFN-γ (I) and in the lysates of PMs of *Btk*$^{-/-}$ and *Btk*$^{+/+}$ mice infected with LM (J), with statistical analysis shown on the right.

Data are shown mean ± SD of three independent experiments (B–D, F, and J) or one representative of three independent experiments with similar results. *$p < 0.05$, **$p < 0.01$ (Student's t test).

See also Figure S5.

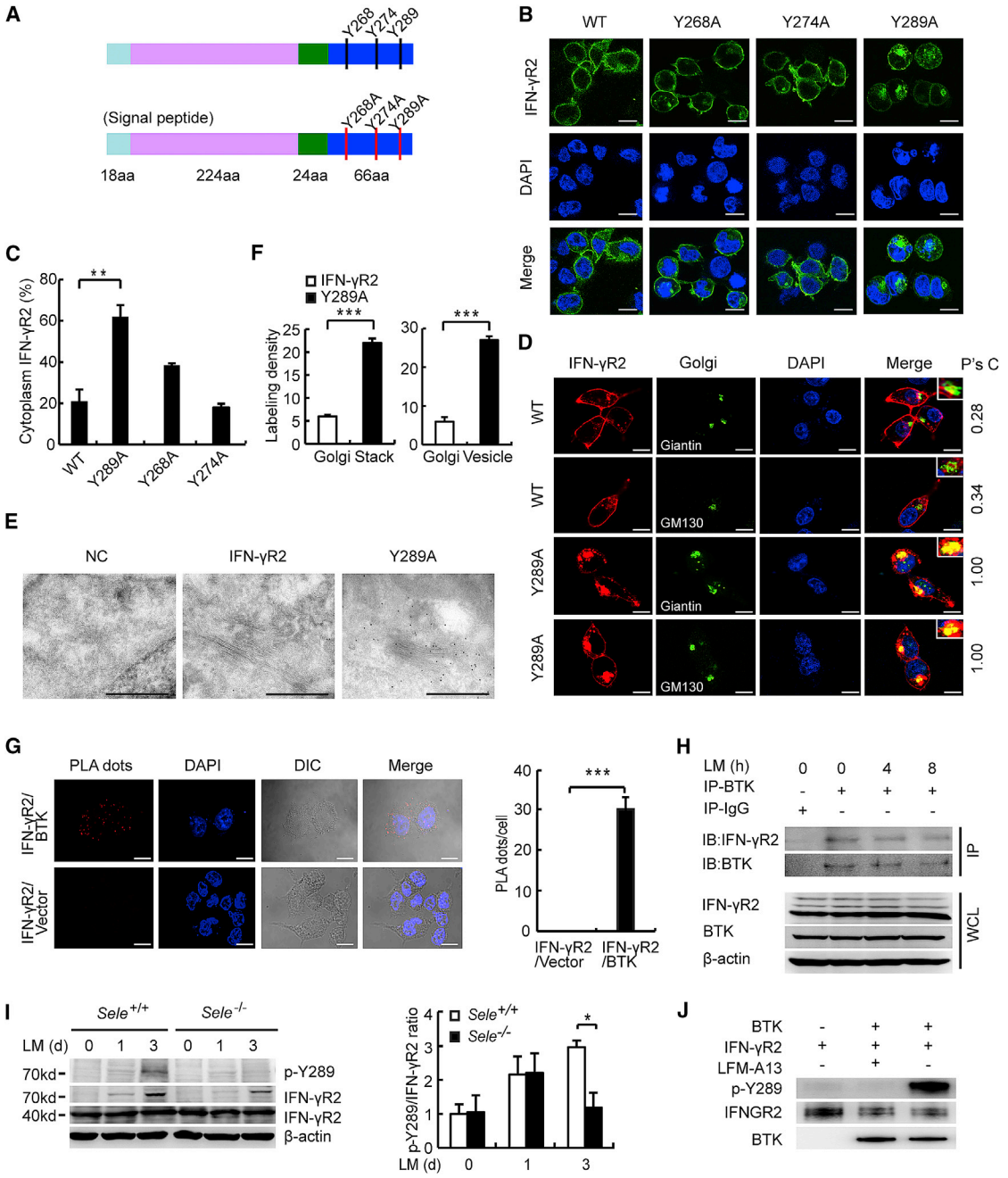

Figure 6. BTK Promotes IFN-γR2 Membrane Translocation by Phosphorylation of IFN-γR2 at Y289

(A) Schematics of full-length and mutation constructs of IFN-γR2.

(B) Confocal microscopy analysis of HEK293T cells transfected with plasmids encoding wild-type or IFN-γR2 mutants. Scale bar, 10 μm.

(C) Quantification of the percentage of cells with cytoplasmic accumulation of IFN-γR2 out of a total of 100 cells in three microscope view fields.

(D) Immunofluorescence staining of IFN-γR2 or IFN-γR2 Y289A and Giantin or GM130 of Golgi in HEK293T cells, Pearson's correlation shown on the right. Scale bar, 10 μm.

(E) Examination of Myc-IFN-γR2 or Myc-IFN-γR2 Y289A location in Golgi of HEK293T cells by immuno-electron microscopy. Scale bar, 500 nm.

(F) Quantification of labeling density of IFN-γR2 or IFN-γR2 Y289A protein in Golgi stacks and vesicles of 35 cells respectively normalized to area.

(G) Representative images and quantification of *in situ* PLA demonstrating the interaction between IFN-γR2 and BTK in HEK293T transfected with IFN-γR2 and BTK plasmids, with the cells transfected with IFN-γR2 and HA-vector as negative control. Scale bar, 10 μm.

(H) IB analysis of endogenous IFN-γR2 in the lysates of PMs stimulated with LM, immunoprecipitated by an antibody to BTK.

(I) IB analysis of p- IFN-γR2 (Y289) expression in lysates of PMs from mice infected with LM (left), statistical analysis was shown on the right.

(legend continued on next page)

was significantly reduced in *Btk*$^{-/-}$ BMDMs stimulated by IFN-γ (Figure 5I). We further observed decreased phosphorylation of JAK1, JAK2, and STAT1 in PMs of *Btk*$^{-/-}$ mice infected with LM *in vivo* (Figure 5J). These data confirm the critical role of E-selectin/BTK signaling in driving cytoplasmic IFN-γR2 translocation to the membrane. We also confirmed the substantially decreased surface levels of IL2Rβ on *Btk*$^{-/-}$ PMs or SMs in response to LM infection (Figures S5G and S5H). In addition, membrane expression of IL2Rβ on RAW 264.7 cells was substantially increased after transfection of BTK compared with control (Figure S5I).

BTK Promotes IFN-γR2 Membrane Translocation via Phosphorylation of IFN-γR2 Tyrosine 289

BTK is a tyrosine kinase, suggesting it may drive IFN-γR2 translocation by phosphorylating IFN-γR2 tyrosine residues. There are eleven tyrosine residues within the IFN-γR2 sequence, three of them, Y268, Y274, and Y289, are located in the intracellular sequence (Figure 6A). These tyrosines are highly conserved between mice and human. We generated three IFN-γR2 mutants, each with one of these three tyrosine residues replaced with alanine (A). IFN-γR2 mutants Y274A and Y268A were located predominantly on the membrane, similar to the wild-type IFN-γR2, while the IFN-γR2 mutant Y289A was accumulated in the cytoplasm (Figures 6B and 6C). IFN-γR2 Y289A co-localized with the Golgi markers Giantin and GM130, indicating its accumulation in the Golgi (Figure 6D). We further performed immuno-electron microscopy (IEM) to observe the subcellular location of wild-type IFN-γR2 and IFN-γR2 Y289A in HEK293T. The results showed that cells transfected with mutant plasmid IFN-γR2Y289A had more colloidal gold in Golgi than cells transfected with wild-type plasmid (Figures 6E and 6F).

We also found that tagged IFN-γR2 and BTK co-localized at the cell membrane in HEK293T cells (Figure S6A), and we further confirmed the direct interaction between IFN-γR2 and BTK in HEK293T by proximity ligation assay (PLA) (Figure 6G). The interaction between endogenous IFN-γR2 and BTK in PMs infected with or without LM was identified by immunoprecipitation with anti-BTK antibody (Figure 6H). We next analyzed whether the activated BTK kinase might phosphorylate Y289 of IFN-γR2 to mediate its membrane translocation. A polyclonal antibody to phosphorylated IFN-γR2 at Y289 was prepared and its specificity was confirmed (Figures S6B and S6C). The phosphorylated IFN-γR2 Y289 (70 kDa) in the cytoplasm increased over time in PMs upon LM infection of *Sele*$^{+/+}$ mice, while this phosphorylation level was lower in PMs from LM-infected *Sele*$^{-/-}$ mice (Figure 6I). Moreover, a cell-free kinase assay revealed that tyrosine 289 of IFN-γR2 was directly phosphorylated by constitutively active BTK (Figure 6J). Therefore, BTK may promote IFN-γR2 translocation from the cytoplasm to the membrane by direct phosphorylation of IFN-γR2 Y289.

EFhd2 Binds to Phosphorylated IFN-γR2 to Drive Its Membrane Translocation

We next investigated whether other molecules are involved in driving the BTK-phosphorylated IFN-γR2 translocation to the membrane. EFhd2 was identified from the proteins immunoprecipitated with an IFN-γR2 antibody by mass spectrometry (Figure S7A). EFhd2 has two EF-hand motifs that can bind calcium (Ca^{2+}) and mediates immune cell activation (Dütting et al., 2011). Ca^{2+} is known to be important for E-selectin-mediated physiological or pathophysiological activities (Chase et al., 2012). We therefore tested if the Ca^{2+}-binding protein EFhd2 interacts with IFN-γR2 to regulate its membrane translocation. First, we found that the Ca^{2+} concentration in the cytoplasm of PMs from *Sele*$^{-/-}$ mice was much lower than that in *Sele*$^{+/+}$ PMs (Figure S7B), which is consistent with reports about Ca^{2+} flux in polymorphonuclear neutrophils elicited by E-selectin signaling (Chase et al., 2012). In the presence of the extracellular Ca^{2+} chelator EGTA or the intracellular Ca^{2+} chelator BAPTA-AM, IFN-γR2 membrane levels were significantly reduced in macrophages upon LM infection (Figure S7C), indicating that E-selectin engagement-induced Ca^{2+} signal is also required to promote IFN-γR2 membrane translocation in macrophages.

EFhd2 was quickly induced in PMs in response to LM infection (Figure S7D). The membrane IFN-γR2 of Efhd2-silenced BMDMs was significantly reduced upon LM infection (Figures 7A and S7E). We also found an interaction between exogenous IFN-γR2 and EFhd2 as well as IFN-γR2 Y289A and EFhd2. Moreover, constitutively activated BTK promoted the interaction between exogenous wild-type IFN-γR2 and EFhd2, but not the interaction between IFN-γR2 Y289A and EFhd2. In addition, we confirmed the interaction between exogenous wild-type BTK and EFhd2 (Figure 7B). Furthermore, the co-localization of IFN-γR2 and EFhd2 in HEK293T cells after co-transfection was confirmed by immunofluorescence (Figure S7F), and we identified direct interaction between IFN-γR2 and EFhd2 in this transfected HEK293T cells by PLA (Figure 7C). Co-immunoprecipitation (coIP) experiments also confirmed that endogenous EFhd2 interacted with IFN-γR2 in PMs (Figure 7D). The endogenous Efhd2 could form a complex with BTK, IFN-γR2, or p-IFN-γR2 in lysates of PMs (Figure 7E).

We next generated *Efhd2* knockout (*Efhd2*$^{-/-}$) mice (Figures S7G and S7H) to determine the role of EFhd2 in driving IFN-γR2 membrane translocation and innate defense *in vivo*. Consistent with the phenotype of *Sele*$^{-/-}$ mice, *Efhd2*$^{-/-}$mice showed significantly decreased expression of IFN-γR2 on the membrane of PMs and impaired LM clearance as compared to their littermate *Efhd2*$^{+/+}$ mice (Figure 7F). There were also significantly increased levels of IFN-γ in the serum of *Efhd2*$^{-/-}$ mice upon LM infection (Figure 7G) and a marked increase in the LM abundance in the spleen and liver of *Efhd2*$^{-/-}$ mice (Figure 7H). The decreased phosphorylation of IFN-γ/JAK-STAT signaling molecules was confirmed in PMs of *Efhd2*$^{-/-}$ mice infected with LM

(J) Cell-free kinase assay of IFN-γR2 phosphorylation at Y289 by constitutively active BTK with or without BTK inhibitor LFM-A13 (100 μM). WCL, whole-cell lysate; DIC, differential interference contrast microscopy.

Data are shown mean ± SD of three independent experiments (C, F, G, and I) or one representative of three independent experiments with similar results. *$p < 0.05$, **$p < 0.01$ (Student's t test).

See also Figure S6.

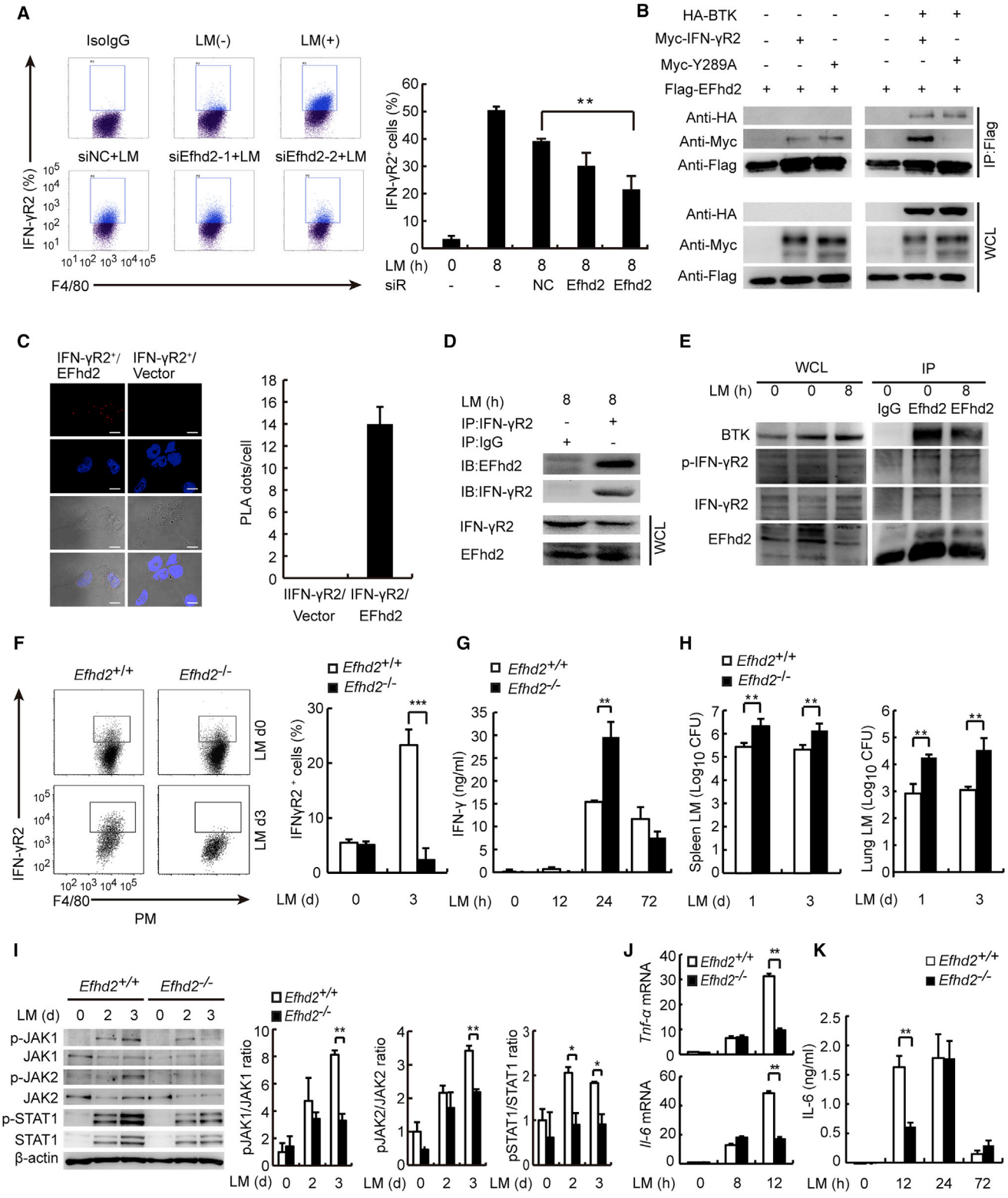

Figure 7. The Calcium-Binding Protein EFhd2 Is Required for Driving Membrane Translocation of IFN-γR2

(A) FACS analysis of surface IFN-γR2 on BMDMs treated with *Efhd2*-specific small interfering RNAs (siRNAs).

(B) Immunoblot analysis of Myc-IFN-γR2/Y289 or HA-BTK in HEK293T cells transfected with indicated plasmids and immunoprecipitated using antibodies to Flag.

(legend continued on next page)

in vivo (Figure 7I). Furthermore, mRNA levels of TNF-α and IL-6 were much lower in PMs of LM-infected *Efhd2*$^{-/-}$ mice than that in the *Efhd2*$^{+/+}$ mice (Figure 7J). Decreased IL-6 protein was observed in sera of *Efhd2*$^{-/-}$ mice infected with LM *in vivo* (Figure 7K).

Taken together, we show that EFhd2 interaction with BTK-phosphorylated IFN-γR2 drives membrane translocation of IFN-γR2, leading to the functional IFN-γR formation, which mediates IFN-γ innate response during LM infection.

DISCUSSION

IFN-γR2 is the subunit-mediated signaling transduction of IFN-γ, and its spatiotemporal distribution and dynamics at cell surface are strictly regulated in immune cells. Multiple mutations have been identified in the human IFN-γR2 gene in patients with MSMD, which lead to complete or partial IFN-γR2 deficiency (Kong et al., 2013). The frequent mutations of IFN-γR2 in MSMD patients further highlight the value of understanding how IFN-γR2 trafficking and maturation are tightly regulated. A series of studies in T cells has confirmed internalization resulted in low or absence of membrane IFN-γR2 (Bernabei et al., 2001), although these T cells display high cytoplasmic IFN-γR2 levels (Rigamonti et al., 2000). These studies suggested that intracellular trafficking determined the location of this subunit in T cells. Many factors may affect the receptor expression on cell membrane such as dynamic neo-synthesis, endocytosis, recycling, and degradation. We did not find reduced synthesis of IFN-γR2 in PMs of *Sele*$^{-/-}$ mice. In addition, our data showed that the degradation process was not involved in the regulation of membrane IFN-γR2 by E-selectin. We further confirmed that the ratio of endocytosis and recycling of IFN-γR2 were not affected after *Sele* deletion. Our data showed that endothelial E-selectin engagement promotes IFN-γR2 translocation from Golgi to the plasma membrane in macrophages, promoting membrane accumulation of IFN-γR2. In addition to colocalization with Golgi, we also found staining of IFN-γR2 in a few other compartments of the cytoplasm in *Sele*$^{-/-}$ macrophages. As synthesis, processing, and translocation of IFN-γR2 are dynamic processes, IFN-γR2 localization or accumulation to some extent in additional compartments such as ER is possible after the deletion of *Sele,* and future investigation will shed more light on this observation.

Importantly, we confirmed the function of E-selectin in regulating IFN-γR2 membrane localization is cell extrinsic. Therefore the processes of macrophages migration from vessels to inflammatory tissues connect the activation of the innate immune cells. E-selectin engages counter-ligands on leukocytes such as PSGL-1, CD44 (Hidalgo et al., 2007), Mac-1 (Crutchfield et al., 2000), CD43 (Matsumoto et al., 2008), and other unknown ligands. We found that E-selectin signal in driving IFN-γR2 membrane translocation was independent of PSGL-1 and Mac-1. There are likely still other unknown ligands on macrophages that are involved in this process (Chase et al., 2012; Hidalgo et al., 2007), which we will continue to investigate in the future.

E-selectin engagement promotes the assembly of functional IFN-γR2 by driving membrane translocation of IFN-γR2 via BTK kinase. BTK is a member of the Tec family and is involved in many signaling pathways via E-selectin (Mueller et al., 2010), B cell receptor (BCR) (Kim et al., 2017), TLR (Liu et al., 2011), or chemokine receptors CXCR4 (de Gorter et al., 2007). BTK-deficient mice have a leukocyte recruitment defect in complex disease models (Mangla et al., 2004). Our study expands the knowledge about the multifaceted role of BTK in immunity and inflammation. A multitude of studies have shown that post-translational modifications (PTM) including phosphorylation, glycosylation, and sumoylation regulate the activation of receptor signaling pathway, recycling, and trafficking (Stone et al., 2017). We found that phosphorylation of IFN-γR2 at Y289 by BTK was critical for membrane accumulation of IFN-γR2 on macrophages. Given the extensive crosstalk between different PTMs, it will be interesting to determine for instance whether phosphorylation of IFN-γR2 Y289 has an effect on the glycosylation of IFN-γR2.

Regulation of the trafficking of membrane receptors has emerged as a key mechanism in controlling signaling output triggered by various inflammatory cytokines and chemokines, leading to a diversity of effects on immune responses. For example, IL-36 ligation induces IL-36R accumulation in lysosomes via a clathrin-mediated pathway, while the ubiquitin-binding Tollip protein increases the accumulation of both subunits of IL-36R to amplify IL-36R signaling (Saha et al., 2015). Transforming growth factor β (TGF-β) receptor type I (TβRI) interacts with SH3 domains of the adaptor protein CIN85, which functions to increase the amount of TβRI at the cell surface and thereby positively regulates TGF-β-stimulated signaling and cell migration (Yakymovych et al., 2015). The translocation of cytokine receptors is associated with pathogenesis and even serves as a potential biomarker and/or therapeutic target for immune diseases, as exemplified by the increased membrane translocation of IL-33R

(C) Representative images (left) and quantification (right) of *in situ* PLA demonstrating the interaction between IFN-γR2 and EFhd2 in HEK293T transfected with IFN-γR2 and EFhd2 plasmids. Scale bar, 10 μm.
(D) IB analysis of endogenous EFhd2 in PMs lysates immunoprecipitated by IFN-γR2 antibody.
(E) IB analysis of endogenous BTK or IFN-γR2 in PMs lysates immunoprecipitated by EFhd2 antibody.
(F) FACS analysis of surface IFN-γR2 on PMs of *Efhd2*$^{+/+}$ or *Efhd2*$^{-/-}$ mice infected with LM for 3 days (n = 5 per group). Quantitative results are shown on the right.
(G) ELISA of IFN-γ in sera.
(H) CFUs in spleens and lungs (n = 5 per genotype).
(I) IB analysis of JAK/STAT molecules in PMs lysates from *Efhd2*$^{+/+}$ or *Efhd2*$^{-/-}$ mice infected with LM, quantification is shown on the right.
(J) *Tnf-α* and *Il-6* mRNAs in PMs were determined by qRT-PCR.
(K) ELISA of IL-6 in sera. Data are shown mean ± SD of three independent experiments (A, C, and F–K) or one representative of three independent experiments with similar results. **p < 0.01, ***p < 0.001 (Student's t test).
See also Figure S7.

in ventilator-induced lung injury (Yang et al., 2015). Here, we report an E-selectin-dependent signaling in driving IFN-γR2 translocation from Golgi to membrane. Moreover, other receptors on macrophage membrane, such as IL2R2 and TLR4, are also dependent on E-selectin signaling in response to LM stimulation. Our findings suggest a broad and critical role for E-selectin signaling and non-immune and immune cell crosstalk in controlling the biological functions of immune cell receptors. It will be intriguing to study whether E-selectin signaling utilizes similar mechanisms as with IFN-γR2 regulation to affect IL-2R2 and TLR4 expression. Our findings also further reveal how host stromal cell and innate immune cell interactions signal to regulate cytokine receptors.

We identified EFhd2, a Ca^{2+}-binding protein that interacts with IFN-γR2 and promotes membrane translocation of IFN-γR2 in activated macrophages. It was previously shown that EFhd2 controls B cell signaling by assembly of the B cell receptor, SYK and PLCγ2 in membrane rafts to promote tyrosine phosphorylation of SYK and PLCγ2 (Kroczek et al., 2010). We now show that EFhd2 interacts with IFN-γR2 to promote its membrane translocation in a Ca^{2+}-dependent manner in response to LM infection. Further investigations are warranted to uncover the detailed mechanisms for EFhd2 regulation of cytokine receptor assembly and cytokine signaling in immunity and inflammation.

STAR★METHODS

Detailed methods are provided in the online version of this paper and include the following:

SUPPLEMENTAL INFORMATION

Supplemental Information includes seven figures and can be found with this article online at https://doi.org/10.1016/j.cell.2018.09.011.

ACKNOWLEDGMENTS

We thank Drs. Ying Li and Xiaofeng Hu at Tsinghua University for Tokuyasu cryosectioning and TEM imaging. This work was supported by the National Natural Science Foundation of China (81788101, 31390431, 31270945, 91542204), National Key R&D program of China (2018YFA0507403), and CAMS Innovation Fund for Medical Sciences (2016-12M-1-003).

AUTHOR CONTRIBUTIONS

X.C. designed the experimental approach and supervised the study. X.X. and J.X. performed the FACS analysis, sorting cells, immunofluorescence, IEM, PLA, HSC transplantation, and animal experiments. J.W. performed the detection of qPCR, western blot analysis, and ELISA. Y. Hu performed isolation and examination of organelles. Y. Han, Y.G., K.Z., and X.L. detected the genotype of knockout mouse. Q.Z. and J.L. performed microarray analysis. B.L. guided BMT experiments. X.X. and X.C. analyzed data and wrote the paper.

DECLARATION OF INTERESTS

The authors declare no competing interests.

Received: September 9, 2017
Revised: August 4, 2018
Accepted: September 7, 2018
Published: October 11, 2018

REFERENCES

Bach, E.A., Szabo, S.J., Dighe, A.S., Ashkenazi, A., Aguet, M., Murphy, K.M., and Schreiber, R.D. (1995). Ligand-induced autoregulation of IFN-gamma receptor beta chain expression in T helper cell subsets. Science *270*, 1215–1218.

Bach, E.A., Aguet, M., and Schreiber, R.D. (1997). The IFN γ receptor: a paradigm for cytokine receptor signaling. Annu. Rev. Immunol. *15*, 563–591.

Benci, J.L., Xu, B., Qiu, Y., Wu, T.J., Dada, H., Twyman-Saint Victor, C., Cucolo, L., Lee, D.S., Pauken, K.E., Huang, A.C., et al. (2016). Tumor interferon signaling regulates a multigenic resistance program to immune checkpoint blockade. Cell *167*, 1540–1554.

Bernabei, P., Coccia, E.M., Rigamonti, L., Bosticardo, M., Forni, G., Pestka, S., Krause, C.D., Battistini, A., and Novelli, F. (2001). Interferon-gamma receptor 2 expression as the deciding factor in human T, B, and myeloid cell proliferation or death. J. Leukoc. Biol. *70*, 950–960.

Bernabei, P., Bosticardo, M., Losana, G., Regis, G., Di Paola, F., De Angelis, S., Giovarelli, M., and Novelli, F. (2003). IGF-1 down-regulates IFN-gamma R2 chain surface expression and desensitizes IFN-gamma/STAT-1 signaling in human T lymphocytes. Blood *102*, 2933–2939.

Blouin, C.M., and Lamaze, C. (2013). Interferon gamma receptor: the beginning of the journey. Front. Immunol. *4*, 267.

Blouin, C.M., Hamon, Y., Gonnord, P., Boularan, C., Kagan, J., Viaris de Lesegno, C., Ruez, R., Mailfert, S., Bertaux, N., Loew, D., et al. (2016). Glycosylation-dependent IFN-gammaR partitioning in lipid and actin nanodomains is critical for JAK activation. Cell *166*, 920–934.

Brubaker, S.W., Bonham, K.S., Zanoni, I., and Kagan, J.C. (2015). Innate immune pattern recognition: a cell biological perspective. Annu. Rev. Immunol. *33*, 257–290.

Chase, S.D., Magnani, J.L., and Simon, S.I. (2012). E-selectin ligands as mechanosensitive receptors on neutrophils in health and disease. Ann. Biomed. Eng. *40*, 849–859.

Chen, W., Han, C., Xie, B., Hu, X., Yu, Q., Shi, L., Wang, Q., Li, D., Wang, J., Zheng, P., et al. (2013). Induction of Siglec-G by RNA viruses inhibits the innate immune response by promoting RIG-I degradation. Cell *152*, 467–478.

Chen, K., Liu, J., Liu, S., Xia, M., Zhang, X., Han, D., Jiang, Y., Wang, C., and Cao, X. (2017). Methyltransferase SETD2-mediated methylation of STAT1 is critical for interferon antiviral activity. Cell *170*, 492–506.e14.

Crutchfield, K.L., Shinde Patil, V.R., Campbell, C.J., Parkos, C.A., Allport, J.R., and Goetz, D.J. (2000). CD11b/CD18-coated microspheres attach to E-selectin under flow. J. Leukoc. Biol. *67*, 196–205.

de Gorter, D.J., Beuling, E.A., Kersseboom, R., Middendorp, S., van Gils, J.M., Hendriks, R.W., Pals, S.T., and Spaargaren, M. (2007). Bruton's tyrosine kinase and phospholipase Cgamma2 mediate chemokine-controlled B cell migration and homing. Immunity *26*, 93–104.

Dütting, S., Brachs, S., and Mielenz, D. (2011). Fraternal twins: Swiprosin-1/EFhd2 and Swiprosin-2/EFhd1, two homologous EF-hand containing calcium binding adaptor proteins with distinct functions. Cell Commun. Signal. *9*, 2.

Gomez, J.A., Wapinski, O.L., Yang, Y.W., Bureau, J.F., Gopinath, S., Monack, D.M., Chang, H.Y., Brahic, M., and Kirkegaard, K. (2013). The NeST long ncRNA controls microbial susceptibility and epigenetic activation of the interferon-γ locus. Cell *152*, 743–754.

Gromova, K.V., Muhia, M., Rothammer, N., Gee, C.E., Thies, E., Schaefer, I., Kress, S., Kilimann, M.W., Shevchuk, O., Oertner, T.G., and Kneussel, M. (2018). Neurobeachin and the kinesin KIF21B are critical for endocytic recycling of NMDA receptors and regulate social behavior. Cell Rep. *23*, 2705–2717.

Groux, H., Sornasse, T., Cottrez, F., de Vries, J.E., Coffman, R.L., Roncarolo, M.G., and Yssel, H. (1997). Induction of human T helper cell type 1 differentiation results in loss of IFN-gamma receptor beta-chain expression. J. Immunol. *158*, 5627–5631.

Hidalgo, A., Peired, A.J., Wild, M., Vestweber, D., and Frenette, P.S. (2007). Complete identification of E-selectin ligands on neutrophils reveals distinct functions of PSGL-1, ESL-1, and CD44. Immunity *26*, 477–489.

Hu, X., and Ivashkiv, L.B. (2009). Cross-regulation of signaling pathways by interferon-gamma: implications for immune responses and autoimmune diseases. Immunity *31*, 539–550.

Hu, X., Herrero, C., Li, W.P., Antoniv, T.T., Falck-Pedersen, E., Koch, A.E., Woods, J.M., Haines, G.K., and Ivashkiv, L.B. (2002). Sensitization of IFN-gamma Jak-STAT signaling during macrophage activation. Nat. Immunol. *3*, 859–866.

Kim, E., Hurtz, C., Koehrer, S., Wang, Z., Balasubramanian, S., Chang, B.Y., Müschen, M., Davis, R.E., and Burger, J.A. (2017). Ibrutinib inhibits pre-BCR^{+} B-cell acute lymphoblastic leukemia progression by targeting BTK and BLK. Blood *129*, 1155–1165.

Kong, X.F., Vogt, G., Itan, Y., Macura-Biegun, A., Szaflarska, A., Kowalczyk, D., Chapgier, A., Abhyankar, A., Furthner, D., Djambas Khayat, C., et al. (2013). Haploinsufficiency at the human IFNGR2 locus contributes to mycobacterial disease. Hum. Mol. Genet. *22*, 769–781.

Kroczek, C., Lang, C., Brachs, S., Grohmann, M., Dütting, S., Schweizer, A., Nitschke, L., Feller, S.M., Jäck, H.M., and Mielenz, D. (2010). Swiprosin-1/EFhd2 controls B cell receptor signaling through the assembly of the B cell receptor, Syk, and phospholipase C gamma2 in membrane rafts. J. Immunol. *184*, 3665–3676.

Lammers, K.M., Lu, R., Brownley, J., Lu, B., Gerard, C., Thomas, K., Rallabhandi, P., Shea-Donohue, T., Tamiz, A., Alkan, S., et al. (2008). Gliadin induces an increase in intestinal permeability and Zonulin release by binding to the chemokine receptor CXCR3. Gastroenterology *135*, 194–204.

Liu, X., Zhan, Z., Li, D., Xu, L., Ma, F., Zhang, P., Yao, H., and Cao, X. (2011). Intracellular MHC class II molecules promote TLR-triggered innate immune responses by maintaining activation of the kinase Btk. Nat. Immunol. *12*, 416–424.

Ma, F., Xu, S., Liu, X., Zhang, Q., Xu, X., Liu, M., Hua, M., Li, N., Yao, H., and Cao, X. (2011). The microRNA miR-29 controls innate and adaptive immune responses to intracellular bacterial infection by targeting interferon-γ. Nat. Immunol. *12*, 861–869.

Malek, T.R., and Castro, I. (2010). Interleukin-2 receptor signaling: at the interface between tolerance and immunity. Immunity *33*, 153–165.

Mangla, A., Khare, A., Vineeth, V., Panday, N.N., Mukhopadhyay, A., Ravindran, B., Bal, V., George, A., and Rath, S. (2004). Pleiotropic consequences of Bruton tyrosine kinase deficiency in myeloid lineages lead to poor inflammatory responses. Blood *104*, 1191–1197.

Matsumoto, M., Shigeta, A., Miyasaka, M., and Hirata, T. (2008). CD43 plays both antiadhesive and proadhesive roles in neutrophil rolling in a context-dependent manner. J. Immunol. *181*, 3628–3635.

Mueller, H., Stadtmann, A., Van Aken, H., Hirsch, E., Wang, D., Ley, K., and Zarbock, A. (2010). Tyrosine kinase Btk regulates E-selectin-mediated integrin activation and neutrophil recruitment by controlling phospholipase C (PLC) gamma2 and PI3Kgamma pathways. Blood *115*, 3118–3127.

Oddo, M., Renno, T., Attinger, A., Bakker, T., MacDonald, H.R., and Meylan, P.R. (1998). Fas ligand-induced apoptosis of infected human macrophages reduces the viability of intracellular Mycobacterium tuberculosis. J. Immunol. *160*, 5448–5454.

Pamer, E.G. (2004). Immune responses to Listeria monocytogenes. Nat. Rev. Immunol. *4*, 812–823.

Pernis, A., Gupta, S., Gollob, K.J., Garfein, E., Coffman, R.L., Schindler, C., and Rothman, P. (1995). Lack of interferon gamma receptor beta chain and the prevention of interferon gamma signaling in TH1 cells. Science *269*, 245–247.

Rigamonti, L., Ariotti, S., Losana, G., Gradini, R., Russo, M.A., Jouanguy, E., Casanova, J.L., Forni, G., and Novelli, F. (2000). Surface expression of the IFN-gamma R2 chain is regulated by intracellular trafficking in human T lymphocytes. J. Immunol. *164*, 201–207.

Saha, S.S., Singh, D., Raymond, E.L., Ganesan, R., Caviness, G., Grimaldi, C., Woska, J.R., Jr., Mennerich, D., Brown, S.E., Mbow, M.L., and Kao, C.C. (2015). Signal transduction and intracellular trafficking by the interleukin 36 receptor. J. Biol. Chem. *290*, 23997–24006.

Schoenborn, J.R., and Wilson, C.B. (2007). Regulation of interferon-gamma during innate and adaptive immune responses. Adv. Immunol. *96*, 41–101.

Sharma, V.K., Pai, G., Deswarte, C., Lodha, R., Singh, S., Kang, L.W., Yin, C.C., Casanova, J.L., Bustamante, J., and Kabra, S.K. (2015). Disseminated Mycobacterium avium complex infection in a child with partial dominant interferon gamma receptor 1 deficiency in India. J. Clin. Immunol. *35*, 459–462.

Slot, J.W., and Geuze, H.J. (2007). Cryosectioning and immunolabeling. Nat. Protoc. *2*, 2480–2491.

Stark, G.R., and Darnell, J.E., Jr. (2012). The JAK-STAT pathway at twenty. Immunity *36*, 503–514.

Stenmark, H. (2009). Rab GTPases as coordinators of vesicle traffic. Nat. Rev. Mol. Cell Biol. *10*, 513–525.

Stone, M.J., Hayward, J.A., Huang, C., E Huma, Z., and Sanchez, J. (2017). Mechanisms of regulation of the chemokine-receptor network. Int. J. Mol. Sci. *18*, E342.

Udalova, I.A., Mantovani, A., and Feldmann, M. (2016). Macrophage heterogeneity in the context of rheumatoid arthritis. Nat. Rev. Rheumatol. *12*, 472–485.

Winkler, I.G., Barbier, V., Nowlan, B., Jacobsen, R.N., Forristal, C.E., Patton, J.T., Magnani, J.L., and Lévesque, J.P. (2012). Vascular niche E-selectin regulates hematopoietic stem cell dormancy, self renewal and chemoresistance. Nat. Med. *18*, 1651–1657.

Xia, L., Sperandio, M., Yago, T., McDaniel, J.M., Cummings, R.D., Pearson-White, S., Ley, K., and McEver, R.P. (2002). P-selectin glycoprotein ligand-1-deficient mice have impaired leukocyte tethering to E-selectin under flow. J. Clin. Invest. *109*, 939–950.

Yakymovych, I., Yakymovych, M., Zang, G., Mu, Y., Bergh, A., Landström, M., and Heldin, C.H. (2015). CIN85 modulates TGFβ signaling by promoting the presentation of TGFβ receptors on the cell surface. J. Cell Biol. *210*, 319–332.

Yang, S.H., Lin, J.C., Wu, S.Y., Huang, K.L., Jung, F., Ma, M.C., Wang Hsu, G.S., and Jow, G.M. (2015). Membrane translocation of IL-33 receptor in ventilator induced lung injury. PLoS ONE *10*, e0121391.

Zarbock, A., Abram, C.L., Hundt, M., Altman, A., Lowell, C.A., and Ley, K. (2008). PSGL-1 engagement by E-selectin signals through Src kinase Fgr and ITAM adapters DAP12 and FcR gamma to induce slow leukocyte rolling. J. Exp. Med. *205*, 2339–2347.

STAR★METHODS

KEY RESOURCES TABLE

REAGENT or RESOURCE	SOURCE	IDENTIFIER
Antibodies		
Phospho-Jak1 (Tyr1022/1023) Antibody	Cell signaling Technology	Cat #3331; RRID: AB_2265057
Phospho-Jak2 (Tyr1007/1008) Antibody	Cell signaling Technology	Cat #3771; RRID: AB_330405
Phospho-Stat1 (Ser727) Antibody	Cell signaling Technology	Cat #9177s; RRID: AB_2197983
JAK1 Antibody	Cell signaling Technology	Cat #3332; RRID: AB_2128499
Jak2 (D2E12) XP Rabbit mAb Antibody	Cell signaling Technology	Cat #3230; RRID: AB_2128522
STAT1 Antibody	Cell signaling Technology	Cat #9172; RRID: AB_2198300
E-selectin /CD62E Antibody	R&D systems	Cat #AF575-SP; RRID: AB_2198300
IFN-gamma R beta (M-20) Antibody	Santa cruz biotechnology	Cat #sc-972; RRID: AB_631718
IFN-γR2 Antibody (MOB-4)	Santa cruz biotechnology	Cat #sc-12752
IFN-γR2 Antibody (for western blot)	Abcam	Cat #ab171081
CHOP Antibody	Cell signaling Technology	Cat #5554T
IFN-γR2 (MOB-4)PE Antibody (for FACS)	Santa cruz biotechnology	Cat #sc-12752
EEA1 Antibody	Cell signaling Technology	Cat #2411; RRID: AB_2096814
Anti-Na^+/K^+-ATPase alpha Monoclonal Antibody, Unconjugated, Clone h-3	Santa cruz biotechnology	Cat #sc-48345; RRID: AB_626712
IFN-γR1 (2E2)- Phycoerythrin Antibody	Abcam	Cat #ab95673; RRID: AB_10687930
CD11b Antibody -APC	Biolegend	Cat #101212; RRID: AB_312795
F4/80 Antibody-PE/Cy7	Biolegend	Cat #123114; RRID: AB_893478
CD11c Antibody -APC	BD Biosciences	Cat #550261; RRID: AB_398460
Ia/e Antibody-APC	Biolegend	Cat #107613
CD3 Antibody-FITC	Biolegend	Cat #100203; RRID: AB_312660
NK1.1 Antibody -percp	Biolegend	Cat #108726
CD19 Antibody -percp	BD Biosciences	Cat #551001
CD4 Antibody -PerCP	BD Biosciences	Cat# 553052; RRID:AB_394587
CD8a Antibody -PE	BD Biosciences	Cat #553033; RRID: AB_394571
CCR2 Antibody -APC	R&D systems	Cat #FAB5538A
IL2R2 (CD122) Antibody -PE (for FACS)	Thermo Fisher Scientific	Cat #12-12221-81; RRID: AB_465832
IL2R2 Antibody (for IB)	Santa cruz biotechnology	Cat #sc-393039
CD284 (TLR4) Antibody -PE	Biolegend	Cat #145404; RRID: AB_2561874
CD45.2 Antibody -APC	Biolegend	Cat #109813; RRID: AB_389210
CD45.1 Antibody -AF488	Biolegend	Cat #110705; RRID: AB_313494
Phospho-BTK Antibody	Cell signaling Technology	Cat #87141
Rabbit Anti-Syk, phospho (Tyr525 / Tyr526) Polyclonal Antibody	Abcam	Cat #58575; RRID: AB_882780
Phospho-p38 MAPK (Thr180/Tyr182) (D3F9) XP Rabbit mAb Antibody	Cell signaling Technology	Cat #4511; RRID: AB_2139685
Phospho-I-kappa-B-alpha (Ser32/36) (5A5) Mouse monoclonal Antibody	Cell signaling Technology	Cat #9246; RRID: AB_2267145
Phospho-IKK / (Ser176/180) (16A6) Rabbit mAb Antibody	Cell signaling Technology	Cat #2697; RRID: AB_2079382
Phospho-IKK / (Ser176/180) (16A6) Rabbit mAb Antibody	Cell signaling Technology	Cat #4370; RRID: AB_2315112
Btk (E-9) Antibody	Santa cruz biotechnology	Cat #sc-28387; RRID: AB_626770
SYK Antibody	Cell signaling Technology	Cat #2712S; RRID: AB_10691458

(*Continued on next page*)

Continued

REAGENT or RESOURCE	SOURCE	IDENTIFIER
Anti-p38 MAPK Antibody	Cell signaling Technology	Cat #9212; RRID: AB_330713
Mouse Anti-IkappaB-alpha Amino-terminal Antigen Monoclonal Antibody	Cell signaling Technology	Cat #4814; RRID: AB_390781
Phospho-IKK / (Ser176/180) (16A6) Rabbit mAb antibody	Cell signaling Technology	Cat #2697; RRID: AB_2079382
ERK 1 (K-23) Antibody	Santa cruz biotechnology	Cat #sc-94; RRID: AB_2140110
FLAG-synthetic antibody	Sigma-Aldrich	Cat #F1804; RRID: AB_262044
Anti-Myc-tag mAb antibody	MBL	Cat #M192-3; RRID: AB_11160947
Myc-Tag (71D10) Rabbit mAb antibody	Cell signaling Technology	Cat #2278S; RRID: AB_10693332
HA-Tag (6E2) Mouse mAb Antibody	Cell signaling Technology	Cat #2367S; RRID: AB_10691311
anti-β-Actin Antibody	MBL	Cat #M177-3; RRID: AB_10697039
Mouse Anti-Giantin Monoclonal Antibody	Abcam	Cat #ab37266; RRID: AB_880195
GM130 Antibody	BD Biosciences	Cat #610822; RRID: AB_398141
Rab5 Rabbit antibody	Cell signaling Technology	Cat #3547
Rab7 Rabbit antibody	Cell signaling Technology	Cat #9367S; RRID: AB_1904103
Rab11 Rabbit antibody	Cell signaling Technology	Cat #5589S; RRID: AB_10693925
DyLight 488 Goat anti-mouse IgG (minimal x-reactivity) antibody	Biolegend	Cat #405310; RRID: AB_1575124
Anti-rabbit IgG (H+L), F(ab')2 Fragment (Alexa Fluor 488 Conjugate) antibody	Cell signaling Technology	Cat #4412; RRID: AB_1904025
Anti-mouse IgG (H+L), F(ab')2 Fragment (Alexa Fluor 555 Conjugate) antibody	Cell signaling Technology	Cat #4409; RRID: AB_1904022
Goat anti-mouse colloidal Gold (12nm)	Jackson	Cat #115-205-068; RRID: AB2338730
DyLight 488 Goat anti-hasmter IgG	Biolegend	Cat #405503
EFHD2 Antibody	Sigma-Aldrich	Cat #SAB3500166; RRID: AB_10642664
Bacterial and Virus Strains		
DH5α	Transgen Biotech	Cat #cd201
L. monocytogenes (*L.M.*)	Provided by Dr. H. Shen from University of Pennsylvania School of Medicine, USA	N/A
Chemicals, Peptides, and Recombinant Proteins		
Tunicamycin	Cell signaling Technology	Cat #12819
E-64	Selleck	Cat #66701-25-5
EZ-Link sulfo-NHS-SS-Biotin	Thermo Scientific	Cat #21331
Glutathione	Sigma-Aldrich	Cat #g4251
MG132	Selleck	Cat #S2619
BAY-61-3606	Selleck	Cat #648903-57-5
LFM-A13	Selleck	Cat #244240-24-2
PDTC	Abcam	Cat #ab141406
EGTA	Sigma-Aldrich	Cat #E0396
BAPTA	Sigma-Aldrich	Cat #A1076
Adenosine 5′-triphosphate disodium salt (ATP)	Sigma-Aldrich	Cat #A7699-1G
Lipofectamine 3000	Invitrogen	Cat #L3000015
Jetprime	Polyplus	Cat #114-15
Lipofectamine RNAiMax	Invitrogen	Cat #13778150
FuGENE HD	Promega	Cat #E2311/2
Recombinant mouse IFN-γ	Peprotech	Cat #315-05-100
PPNIPEQIEEYLKDPDQFILE	Sangon Biotech	N/A
PPNIPEQIEE {p- Y } LKDPDQFILE	Sangon Biotech	N/A

(*Continued on next page*)

Continued

REAGENT or RESOURCE	SOURCE	IDENTIFIER
E-Selectin/CD62E Fc chimera	R&D systems	Cat #575-ES-100
Recombinant murine M-CSF	Peprotech	Cat #315-02
Monoclonal Anti-HA-Agarose antibody	Sigma-Aldrich	Cat #A2095
Anti-c-Myc Agarose Affinity Gel antibody produced in rabbit	Sigma-Aldrich	Cat #A7470
c-Myc Peptide	Sigma-Aldrich	Cat #M2435
Influenza Hemagglutinin (HA) Peptide	ApexBio	Cat #A6004
Critical Commercial Assays		
Mouse IFN-γ ELISA kit	Biolegend	Cat #430808
Mouse IL-6 ELISA kit	Biolegend	Cat #431308
Mouse TNF-α ELISA kit	Biolegend	Cat #430908
Duolink *In Situ* Red Starter Kit Mouse/Rabbit	Sigma-Aldrich	DUO92101
Murine Plasma Membrane Protein Isolation kit	Invent Biotechnologies	Cat #SM-005
Murine Endosome Isolation and Cell Fractionation kit	Invent Biotechnologies	Cat #ED-028
Golgi Isolation kit	Sigma-Aldrich	Cat #GL0010
ReverTra Ace qPCR RT kit	TOYOBO	Cat #FSQ-101
Deposited Data		
cDNA Microarray raw data	This paper	GEO: GSE90808
cDNA Microarray raw data	This paper	GEO: GSE97790
Experimental Models: Cell Lines		
HEK293T	ATCC	Cat #CRL11268
RAW264.7	ATCC	Cat #TIB-71
Jurkat	ATCC	Cat #TIB-152
U-937	ATCC	Cat #CRL-1593.2
Experimental Models: Organisms/Strains		
Sele deficient (*Sele*$^{-/-}$) mice:(B6.129S2-Sele^{tm2Hyn}/J)	The Jackson Laboratory	JAX stock 008434
Btk deficient (*Btk*$^{-/-}$) mice:B6.129S-BTK^{tm1wk}/J	The Jackson Laboratory	JAX stock 002536
Itgam deficient (*Itgam*$^{-/-}$) mice: B6.129S4-Itgamtm1Myd/J	The Jackson Laboratory	JAX stock 003991
Seleplg deficient (*Seleplg*$^{-/-}$) mice: B6.129-*Selplg*^{tm1Rpmc}/J	The Jackson Laboratory	JAX stock 006336
Prm-Cre mice:129S/Sv-Tg(Prm-cre)58Og/J	The Jackson Laboratory	JAX stock 003328
CD45.1^{+} C57BL/6 mice: B6.SJL-Ptprca Pepcb/BoyJ	The Jackson Laboratory	JAX stock 002014
Efhd2 $^{flx/flx}$ B6.129-mice	This paper	N/A
Oligonucleotides		
siRNA: *Syk*: 5′-GGCAGCUAGUGGAACAUUATT-3′ (sense)	Genepharma	N/A
siRNA: *Btk*: 5′-CAUCACCUUUAAACUUCAATT-3′ (sense)	Genepharma	N/A
siRNA: *p65*: 5′-CUCAAGAUCUGCCGAGUAATT-3′ (sense)	Genepharma	N/A
siRNA: *Efhd2-1*: 5′-CCAGGAAGCAGAUCAAAGATT-3′ (sense)	Genepharma	N/A
siRNA: *Efhd2-2*: 5′-GCCGCUUUGAGGAAGAGAUTT-3′ (sense)	Genepharma	N/A
Ifngr2 gRNA-1: 5′-ACCGTGCCACATATGATAGATGG-3′	Sangon Biotech	N/A
Ifngr2 gRNA-1: 5′-ACCGTTCAGTGAGTGTCCTTGCTG-3′	Sangon Biotech	N/A
Primer: Ifngr2 (Fw): 5′- CAGCAAGTCATCCTGATTCC −3′	Sangon Biotech	N/A
Primer: *Ifngr2* (Rev): 5′- CTGGGTCCTTTAGATACTCT-3′	Sangon Biotech	N/A

(*Continued on next page*)

Continued

REAGENT or RESOURCE	SOURCE	IDENTIFIER
Primer: *Sele* (Fw): 5′- GTCTAGCGCCTGGATGAAAG −3′	Sangon Biotech	N/A
Primer: *Sele* (Rev): 5′- ATTGCCACCAGATGTGTGTA −3′	Sangon Biotech	N/A
Primer: *Tnfα* (Fw): 5′- AAGCCTGTAGCCCACGTCGTA −3′	Sangon Biotech	N/A
Primer: *Tnfα* (Rev): 5′-GCCACCACTAGTTGGTTGTC TTTG −3′	Sangon Biotech	N/A
Primer: *Il6* (Fw): 5′- TAGTCCTTCCTACCCCAATTTCC −3′	Sangon Biotech	N/A
Primer: *Il6* (Rev): 5′- TTGGTCCTTAGCCACTCCTTC −3′	Sangon Biotech	N/A
Primer: *Ifngr2* KO (Fw): 5′- TGATTTGTGGCTCTCA GGG −3′	Sangon Biotech	N/A
Primer:*Ifngr2* KO (Rev): 5′- AGATGAGCAGGAGGT GATG −3′	Sangon Biotech	N/A
Recombinant DNA		
Plasmid: pcDNA3.1-myc	Invitrogen	Cat #V855-20
Plasmid: pcDNA3.1-flag	This paper	N/A
Plasmid: pcDNA3.1-ha	This paper	N/A
Plasmid: pcDNA3.1-*Btk*-ha	This paper	N/A
Plasmid: pcDNA3.1-*Btk*K42R-ha	This paper	N/A
Plasmid: pcDNA3.1-*Ifngr2*-myc	This paper	N/A
Plasmid: pcDNA3.1-*Ifngr2*Y289A-myc	This paper	N/A
Plasmid: pcDNA3.1-*Efhd2*-flag	This paper	N/A
Plasmid: pGL3-U6-sgRNA-PGK-puromycin	Addgene	Cat #51133
Plasmid:pST1347-NLS-flag-linker-Cas9	Addgene	N/A
Software and Algorithms		
FACSDiva software	BD Bioscience	http://www.bdbiosciences.com/us/instruments/research/software/flow-cytometry-acquisition/bd-facsdiva-software/m/111112/overview
ImageJ	NIH	https://imagej.nih.gov/ij/download.html
FV10-ASW 3.0 Viewer	PHOTONICS MEDIA	https://www.photonics.com/Product.aspx?PRID=47380
ZEN lite software	ZEISS	https://www.zeiss.com/microscopy/int/products/microscope-software/zen-lite.html
Other		
Kinase buffer	Cell signaling Technology	Cat #9802

CONTACT FOR REAGENT AND RESOURCE SHARING

Further information and requests for resources and reagents should be directed to and will be fulfilled by the Lead Contact, Xuetao Cao (caoxt@immunol.org)

EXPERIMENTAL MODEL AND SUBJECT DETAILS

Mice

Sele deficient (*Sele*$^{-/-}$) mice:(B6.129S2-Sele^{tm2Hyn}/J), *Btk* deficient (*Btk*$^{-/-}$) mice: B6.129S-BTK^{tm1wk}/J, *Itgam* deficient (*Itgam*$^{-/-}$) mice: B6.129S4- Itgamtm1Myd/J, *Seleplg* deficient (*Seleplg*$^{-/-}$) mice: B6.129-*Selplg*^{tm1Rpmc}/J, Prm-Cre mice: 129S/Sv-Tg(Prm-cre)58Og/J and CD45.1^{+} C57BL/6 mice: B6.SJL-Ptprca Pepcb/BoyJ were obtained from The Jackson Laboratory. *Efhd2* $^{flx/flx}$ mice were generated by Bacterial Artificial Chromosomes (BAC) recombineering technology. *Efhd2* $^{flx/flx}$ mice were generated as follows: The second exon of *Efhd2* was flanked by loxp, and loxp, neo and frt were located in the introns next to second exon, and a frameshift leads to early termination of translation after deletion of floxp region by cre. The targeting vector pBR322-MK-*Efhd2* for

generating the *Efhd2*$^{f/f}$ allele was obtained and transfected in ES cells by electroporation. ES cells obtained by positive-negative selection with G418 and Ganciclovoir were identified by PCR. The selected ES cells were injected into C57BL/6 blastocysts, and then the embryo was transferred into the pseudo pregnant uterus of C57BL/6 to obtain a chimeric mouse. PCR was performed to identify a heterozygous mouse from the offspring arising from breeding the chimeric mouse with C57BL/6 using the same primers as were used for ES identification. The heterozygous mouse *Efhd2*$^{f/neo/+}$ was crossed with B6; SJL-Tg (ACTFLPe) 9205Dym/J (JAX: 003800) was used to delete the PGK-neo box to obtain the *Efhd2*$^{f/+}$ mouse. We further bred the *Efhd2*$^{f/+}$ mouse with 129S/Sv-Tg (Prm-cre)58Og/J (JAX:003328), which has a *cre* target transgene only in the male germline, to get a *Efhd2*$^{+/-}$ mouse, and this mouse was then backcrossed with C57BL/6 for 8 generations to get *Efhd2*$^{-/-}$ mouse, which background is transferred into C57BL/6. We used 6-week old littermate mice (matched for body weight and sex) in our experiments. All animal experiments were approved by the Animals Care and Use Committees of the Institute of Laboratory Animal Sciences of Chinese Academy of Medical Sciences (ILAS-GC-2015-002).

Culture and Maintenance of Cell

Thioglycolate-elicited mouse PMs were prepared and cultured in endotoxin-free RPMI-1640 medium with 10% (vol/vol) FCS (Invitrogen) as described previously (Chen et al., 2017). BM-derived macrophages from C57BL/6 mouse were generated by culturing of BM cells with M-CSF (50ng/ml) for 5 days (Peprotech) as described previously (Chen et al., 2013). The HEK293T, RAW264.7, Jurkat and U-937 cell lines were from American Type Culture Collection. The cells were cultured in endotoxin-free DMEM (GIBICO) supplemented with 10% FCS.

METHOD DETAILS

Bacterial Culture, Infection, and Quantification

LM in mid-logarithmic growth were collected, counted on agar plates, and then re-suspended in PBS. Mice were i.p. injected with 1×10^8 or 1×10^7 LM. At indicated times following infection, mouse survival was monitored after infection with 1×10^8 LM, and spleens and livers were harvested from mouse infected with 1×10^7 LM and then dissociated in PBS containing 0.05% Triton X-100 for measurement of colony-forming units as described previously (Ma et al., 2011). Bone marrow-derived macrophages in 6-well plates were stimulated with inactivated 1×10^8 LM per well for 12 hours.

RNA Quantification

Quantitative PCR analysis was performed by LightCycler (Roche) using a SYBR RT-PCR kit (Takara) as described previously (Chen et al., 2017). Data were normalized to β-actin expression.

ELISA

The concentrations of IL-6, TNF-α, and IFN-γ in the sera were measured by ELISA kits (R&D Systems).

Microarray Analysis

Total RNA was isolated using an RNA isolation Kit (Ambion, Austin, TX, USA). Affymetrix Mouse Genome 430 2.0 Arrays were used to analyze genome-wide expression. Detailed procedures were as described previously (Chen et al., 2013).

Flow Cytometry and Intracellular Cytokine Staining

Cells were resuspended at 1×10^6/ml in 5% rat serum containing PBS, and surface staining was performed as described previously (Chen et al., 2013). For intracelluar cytokine staining, splenocytes or PMs from mice infected with LM for 3 days *in vivo* were stained with the Cytofix/Cytoperm kit (ebioscience) following the manufacturer's instructions. Cells were analyzed by flow cytometer (BD LSRII or BD FACSVerse).

Immunofluorescence

PMs from mice infected with LM for 3 days were plated and fixed on the glass coverslips in 24-well plates, then the primary antibodies (Giantin, IFN-γR2, Rab7, Rab5, Rab11) were incubated with the cells without permeabilization at room temperature for 90 min as described (Lammers et al. [2008] and the protocol of PD-1 on website https://www.abcam.cn/pd1-antibody-epr20665-ab214421.html). The cells were washed with PBS two times, add second antibody directly to the center of the coverslip, incubated for 30 minutes at room temperature. After screening for antibodies to stain cytoplasmic proteins using the protocol without permeabilization, we used antibodies against rab5, rab7 and rab11 from CST and giantin from Abcam to do the experiments.

HEK293T cells transfected with constructs were plated on the glass coverslips in 24-well plates, and the cells were labeled with antibodies against Flag-tag, Myc-tag, HA-tag after fixation and permeabilization. The cells were washed with PBS two times, second antibody was added directly to the center of the coverslip, incubated for 30 minutes at room temperature. Cells were subjected to microscopy analysis with the Olympus FV100 or Zeiss LSM780 confocal laser microscope. We analyzed Pearson's index based on the Golgi area VS IFN-γR2 (red to green in primary microphages, green to red in HEK293T) when we clarify colocalization between Golgi and IFN-γR2.

Immunoprecipitation, Immunoblot, and Immunohistochemistry

Cells were lysed with cell lysis buffer (CST) supplemented with protease inhibitor cocktail (Calbiochem). Protein concentrations of the extracts were measured with BCA assay (Pierce). Immunoprecipitation and immunoblot assays were performed as described previously (Chen et al., 2017). Paraffin sections of spleen tissue were prepared as described (Chen et al., 2013) and immunohistochemically incubated with E-selectin antibody using ABC kit (Pierce).

RNA Interference

SiRNAs were transfected using RNAi MAX reagent (Invitrogen) at a final concentration of 20 nM following the manufacturer's instructions. The efficiency of interference was identified by qRT-PCR or western blot.

Generation of Ifngr2-KO RAW264.7 Cells

The *Ifngr2* knockout (KO) RAW264.7 cells were generated by using the CRISPR/Cas9 gene-editing system. We transfected RAW264.7 cells with Cas9 and sgRNA expressing plasmids as described before, blasticidin S hydrochloride (2 μg/mL; Life Technology) and puromycin (3 μg/mL; Life Technology) were added after transfection 24 h, detection of mutation by PCR and DNA sequencing were performed in the DNA of cell clones, and then we confirmed *Ifngr2* knockout by western blot and FACS analysis.

Isolation of Membrane, Endosome and Golgi

Membrane

Murine Plasma Membrane Protein Isolation kit (Invent Biotechnologies) was used to isolate membrane according to the manufacturer's instruction. Briefly, 5 × 10^7 cells were collected and added buffer A, and then incubate the cell suspension on ice for 10 min. Then gradient centrifugation was performed.

Endosome

Murine Endosome Isolation and Cell Fractionation kit (Invent Biotechnologies) was used to isolate endosome according to the manufacturer's instruction. Briefly, 5 × 10^7 cells were collected and added buffer A. Then the cell suspension was incubated on ice for 10 min. Filter cartridge filled with cell suspension was centrifuged. The pellet was resuspended, and the supernatant was transferred to a fresh tube, and the tube added 500ul buffer B was incubated at 4°C for 4h. Remove the supernatant and save the pellet in buffer WA-009 after centrifugation.

Golgi:

Golgi isolation kit (Sigma-Alorich) was used to isolate endosome according to the manufacturer's instruction. Briefly, 5 × 10^7 cells were collected and washed in ice-cold PBS, 0.25M sucrose solution was added to the cells, then the suspension was homogenized and centrifuged, and then 2.3 M sucrose solution was added to a final sucrose concentration of 1.25 M. Build a discontinuous gradient in an ultracentrifuge tube. Centrifuge the tubes at 120,000 × g for 3 hours at 4°C. Withdraw the Golgi enriched fraction from 1.1/0.25M sucrose interphase.

Examination of IFN-γR2 Endocytosis and Recycling

Cell surface protein was labeled with EZ-Link Sulfo-NHS-SS-Biotin (Thermo Scientific) to examine endocytosis and recycling of IFN-γR2 in peritoneal macrophages described previously (Gromova et al., 2018). Briefly, peritoneal macrophages derived from *Sele*$^{-/-}$ and *Sele*$^{+/+}$ mice were seeded on 3.5cm dishes, and then E64 protease inhibitor was added for 1 h at 37°C to prevent lysosomal proteolysis of internalized IFN-γR2. The cells were rinsed twice in ice-cold PBS, and then cold PBS with 0.4 mM Fresh EZ-Link Sulfo-NHS-SS-Biotin was added to the cells for 20 min at 4°C. Cells were washed by quenching buffer to remove unreacted biotin. To examine the internalization of labeled receptors, cells were incubated in medium containing E64 at 37°C for 30 min. Biotin labeled on surface receptors were cleaved with glutathione cleavage buffer at 4°C. RIPA with protease inhibitors was added to cells washed with ice cold PBS. To examine the recycling of internalized receptors to membrane, cells treated with glutathione cleavage buffer after internalization were incubated in medium containing E64 at 37°C for 1h, and then repeat the cleavage. Cells were harvested with RIPA. Western blot was performed after precipitation of biotin-labeled receptors by streptavidin-dynabeads (Invitrogen).

E-selectin Adhesion Assays and E-selectin Engagement on Peritoneal Macrophages (PMs)

For static adhesion assays, 96-well plates were coated with purified recombinant mouse E-selectin–human IgG1 (huIgG1)-Fc fusion proteins overnight at 4°C (R&D Systems, 4 ug/ml with 100 μL/well). Jurkat or U937 cells were added to each of triplicate selectin- or control-coated wells (5 × 10^4cells/ well). Cells were left in contact with the coated surface for 1-hour incubation, washed four times, and the numbers of adherent cells was quantified.

For E-selectin engagement, 24-well plates were coated with or without purified recombinant mouse E-selectin fusion proteins as described previously. PMs were added to each of triplicated selectin- or control-coated wells (3 × 105 cells/ well). Cells were left in contact with the coated surface for 12 hours in the incubator and then were used for FACS analysis as described previously.

HSC Transplantation

HSC (50 per mouse) sorted from *Sele*$^{+/+}$ (CD45.1^{+}) mice bone marrow and protection cells (5 × 10^{4}) were transplanted into (9.0 Gy) lethally-irradiated *Sele*$^{+/+}$(CD45.2^{+}) or *Sele*$^{-/-}$ (CD45.2^{+}) mice via tail-vein injection. The efficiency of transplantation was analyzed by examination the cells in blood with FACS after 6 weeks, and then the mice were i.p. injected without or with LM and sacrificed on day 3. IFN-γR2 expression on the membranes of macrophages was analyzed by flow cytometry.

Plasmid Constructs

Recombinant vectors encoding mouse IFN-γR2 (NM_008338.3), IFN-γR2 mutants Y268A, Y274A, and Y289A, BTK and constitutively active BTK(NK_013482.2) were constructed by PCR-based amplification from cDNA of mouse macrophages and then subcloned into pcDNA3.1 eukaryotic expression vectors (Invitrogen) as described previously (Chen et al., 2017). All constructs were confirmed by DNA sequencing.

Transfection of Cells

HEK293T, Jurkat and U-937 were cultured in DMEM medium with 10% (vol/vol) FCS. BM-derived macrophages and HEK293T cells (American Type Culture Collection) were transfected with JetPEI reagents (PolyPlus) or FuGENE HD (Promega) according to the manufacturer's instruction.

Generation of Polyclonal Antibody against p-Y289 IFN-γR2

Peptides were synthesized (Sangon Biotech), and the EQIEE(pY)LKDPD peptide was used for immunization, and the EQIEEYLKDPD peptide was used for a negative control. New Zealand white rabbits were immunized with the EQIEE(pY)LKDPD peptide coupled with Freund's complete adjuvant. We administered three booster doses at two-week intervals. Blood was drawn from the immunized rabbit two weeks after the third booster, and the antibody was obtained after affinity purification by using the EQIEE(pY)LKDPD peptide. The titer of the purified antibody was tested by ELISA using the EQIEE(pY)LKDPD peptide, and the EQIEEYLKDPD peptide was used for a negative control.

Immuno-Electron Microscopy

We performed Immuno-electron microscopy as described as previously (Slot and Geuze, 2007). Briefly, HEK293T cells transfected with IFN-γR2 or IFN-γR2Y289A plasmid were pre-fixed in medium plus fixation buffer (2% formaldehyde and 0.01% glutraradehyde in PB buffer) (1:1) for 5 min at room temperature, and then the supernatant was discarded. The cells were fixed in fixation buffer for 1h at room temperature. The cells were washed in dish with chilled PB buffer 5min, 1% gelatin was added in the dish after discarding of supernatant, and then the cells were scraped. Cells were centrifuged 1000 g for 5min and then suspended in 12% gelatin. After incubating at 37°C for 10min, the cells were put on the ice for 15min to solidify the gelatin. Make small blocks about 0.5 mm × 3 mm then immersed the cell blocks in 2.3M sucrose overnight in cold room overnight. Glue the blocks on the pins before freezing in liquid nitrogen. 70nm sections were cut in an ultracryotome at −120 degree (Leica EM FC7). Cell blocks were immunolabled with anti-Myc antibody (MBL, 1:200) for 1.5 hours and then incubate with 12nm Goat anti-mouse colloidal Gold (Jackson,115-205-068) for 40 minutes. The labeled cryosections were viewed under Tecnai spirit 120kv transmission electron microscope (FEI, USA).

In vitro Kinase Assay

Myc-tagged IFN-γR2 expressed in HEK293T cells was immunoprecipitated by anti-c-Myc Agarose Affinity Gel antibody and eluted by c-Myc peptide. In the same way, HA-tagged constitutively active BTK expressed in HEK293T cells was immunoprecipitated by Monoclonal Anti-HA−Agarose antibody and eluted by HA peptide. These two proteins were incubated together in kinase assay buffer (CST) with ATP according to the manufacturer's instructions.

In situ Proximity Ligation Assay

HEK293T cells transfected with plasmids including Myc- IFN-γR2 and Flag-EFhd2 or Myc- IFN-γR2 and Ha-BTK were fixed in 3% paraformaldehyde for 10 min followed by 5 min 0.01% triton-100 PBS, and the cells incubate with the primary antibodies (anti-MYC antibody, MBL M192-3,1:2000; anti-FLAG CST, 1:800) as same as immunofluorescence, and then *in situ* PLA was performed according to the manufacturer's instructions (DUO92101, Sigma-Aldrich), Images were captured with Olympus confocal microscope.

Nanospray Liquid Chromatography-Tandem Mass Spectrometry

RAW264.7 macrophage cells (3 × 10^{8}) were stimulated for 12h with LM, and then the cells were lysed for preparation of immunoprecipitates with anti-IFN-γR2. Proteins were eluted and digested. Digests were analyzed by nana-ultra-performance liquid chromatography-electrospray inonization tandem mass spectrometry. Data from liquid chromatography-tandem mass spectrometry were processed through proteinLynx Global Server version 2.4 (PLGS2.4); the resulting peak lists were used for searching the NCBI protein database with the Mascot search engine.

QUANTIFICATION AND STATISTICAL ANALYSIS

Results were presented as mean and SD. The statistical significance of comparisons between two groups was determined with Student's t test. $p < 0.05$ was taken to indicate statistical significance. The statistical significance of survival curves was estimated according to the method of Kaplan and Meier, and the curves were compared with the generalized Wilcoxon's test.

DATA AND SOFTWARE AVILABILITY

The accession numbers for the cDNA microarray data reported in this paper are GEO: GSE90808 and GSE97790.

Cell

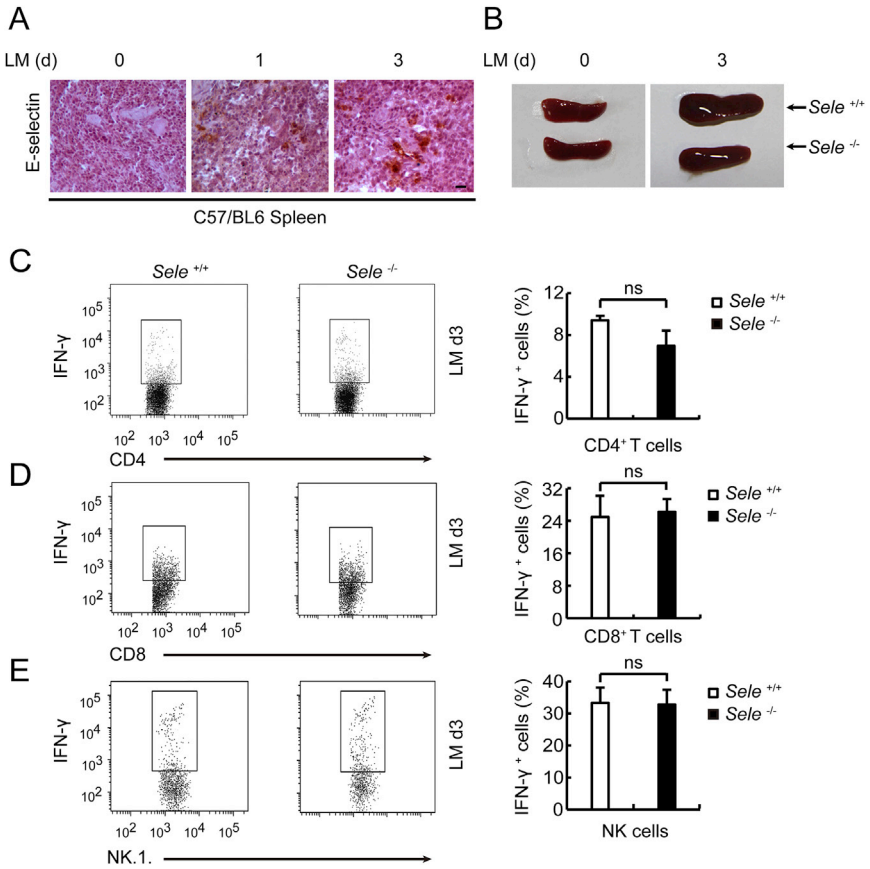

Figure S1. Upregulation of Splenic E-Selectin Expression in Mice Infected with LM and Unchanged Production of IFN-γ by Immune Cells in *Sele*$^{-/-}$ Mice Infected with LM, Related to Figure 1

(A) Analysis of E-selectin protein expression in spleen of LM-infected *Sele*$^{+/+}$ mice for indicated days by immunohistochemistry (Scale bar: 100 μm). (B) The spleen of *Sele*$^{-/-}$ and *Sele*$^{+/+}$ mice infected without or with LM for 3 days. Data are representative of three independent experiments with similar results. (C-E) Intracellular staining of IFN-γ in splenic immune cells, including CD4^{+} T cells (C), CD8^{+} T cells (D), and NK cells (E), of *Sele*$^{-/-}$ and *Sele*$^{+/+}$ mice infected with LM on day 3. Right panel shows the percentage of IFN-γ positive cells. LM: *Listeria monocytogenes*. Data are shown mean ± SD of three independent experiments (right panel of C-E) or one representative of three independent experiments with similar results.

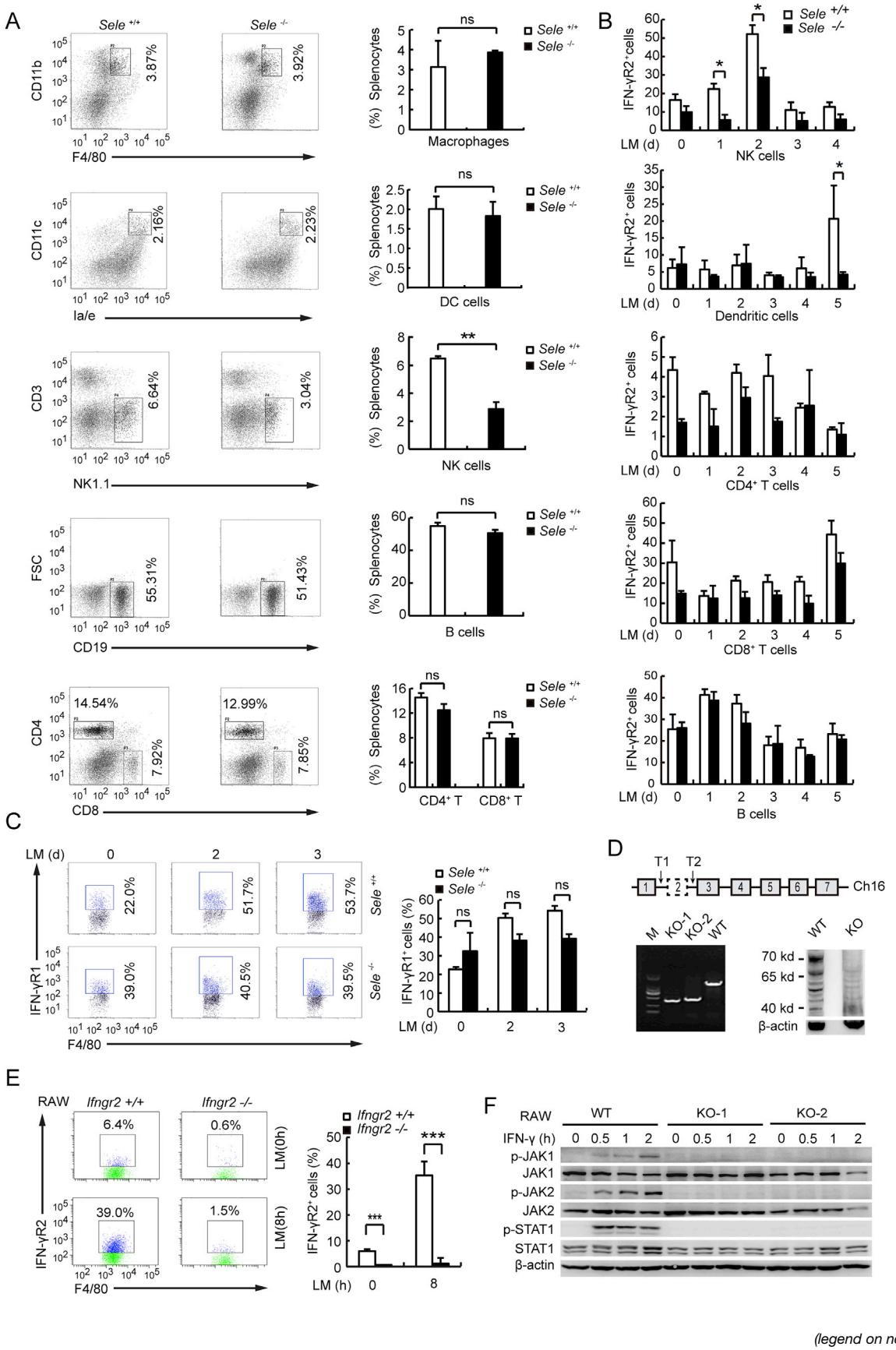

(legend on next page)

Figure S2. Generation of *Ifngr2* Knockout RAW264.7 Cells and Development of Immune Cells in *Sele*$^{+/+}$ and *Sele*$^{-/-}$ Mice, Related to Figure 2

(A) Flow cytometry analysis of the ratio of splenic macrophages, dendritic cells, NK cells, B cells, and CD4^{+} or CD8^{+} T cells of *Sele*$^{-/-}$ and *Sele*$^{+/+}$ mice. Right panels show the ratio of the immune cells. (B) Flow cytometry analysis of IFN-γR2 surface expression on splenic NK cells, DC, CD4^{+} T cells, CD8^{+} T cells, and B cells in *Sele*$^{-/-}$ and *Sele*$^{+/+}$ mice infected with LM for indicated times, the histograms show the percentages of INFGR2 positive cells. (C) IFN-γR1 expression on the membrane of peritoneal macrophages examined by flow cytometry, and quantification analysis shown on the right panel. (D) Schematic diagram showing the target sites used for CRISPR/Cas9 gRNA to generate of *Ifngr2* knockout RAW264.7 cells (up panel), and identification of the *Ifngr2*$^{+/+}$or *Ifngr2*$^{-/-}$ RAW264.7 cells by PCR or western blot (down panel). (E) FACS analysis of IFN-γR2 expression on the membrane of *Ifngr2*$^{+/+}$or *Ifngr2*$^{-/-}$ RAW264.7 cells without or with LM stimulation (left panel), and the quantification analysis shown in the right panel. (F) JAK/STAT signaling molecules in the lysates of *Ifngr2*$^{+/+}$or *Ifngr2*$^{-/-}$ RAW264.7 cells stimulated with IFN-γ (10U/ml) on indicated times were measured by immunoblot analysis. Data are shown mean ± SD of three independent experiments (right panel of B, D, E and F) or one representative of three independent experiments with similar results. *$p < 0.05$, ***$p < 0.001$ (Student's t test).

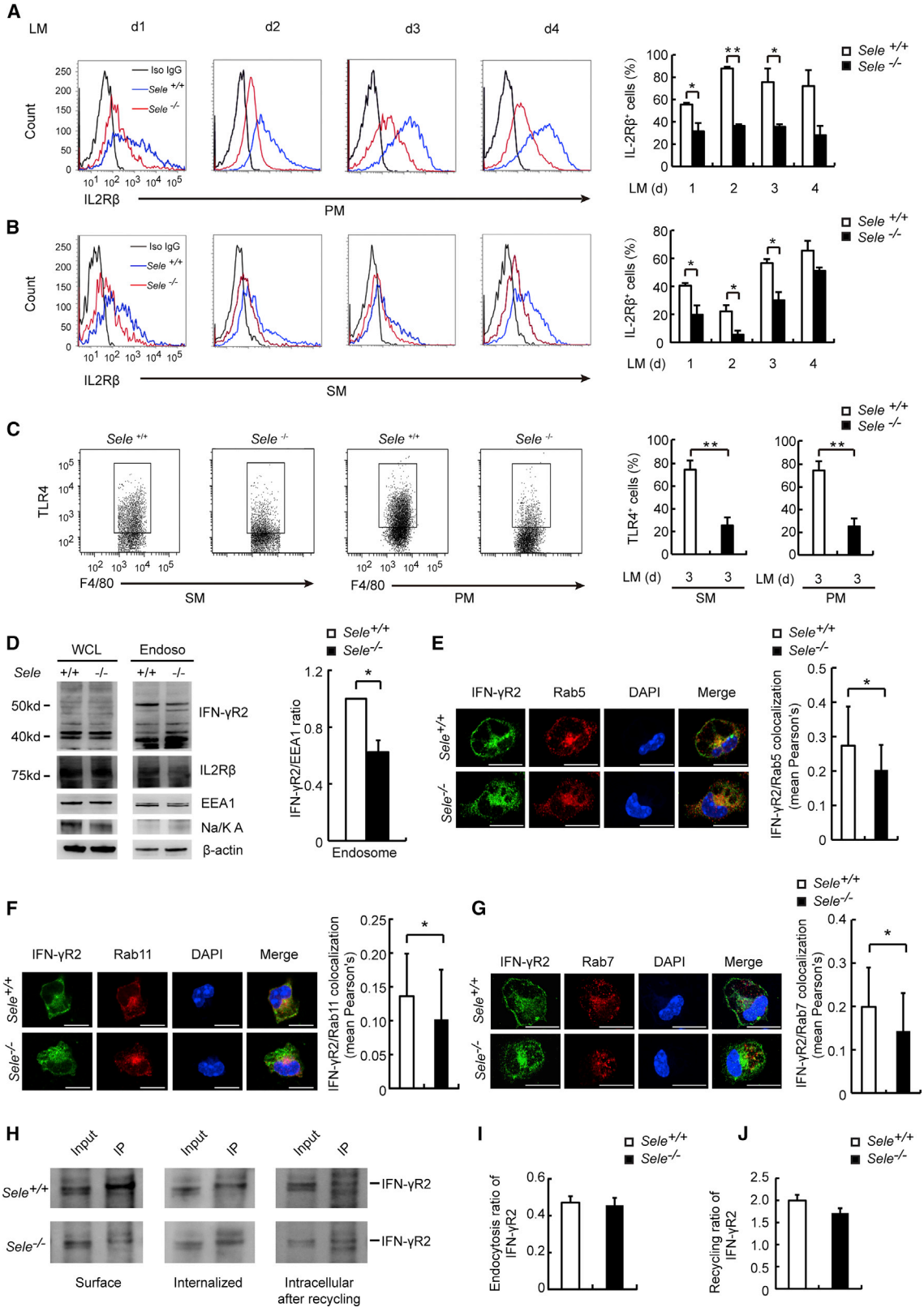

(legend on next page)

Figure S3. Decreased IL-2Rβ or TLR4 Expression on the Membrane of Macrophages in *Sele*$^{-/-}$ Mice, Related to Figure 3

(A-C) Flow cytometry analysis of IL-2Rβ subunit on peritoneal macrophages (A) or splenic macrophages (B) or TLR4 expression on peritoneal macrophages or splenic macrophages (C) from *Sele*$^{+/+}$ or *Sele*$^{-/-}$ mice infected with LM for indicated days. Isotype IgG served as the negative control. (D) IB analysis of IFN-γR2 or IL2Rβ and quantifications of IFN-γR2 in the isolated endosome from *Sele*$^{+/+}$ and *Sele*$^{-/-}$ PMs. All samples were run on the same gel. (E-G) Representative images of immunofluorescence and quantification of colocalization between IFN-γR2 and Rab5 (E), Rab11 (F) or Rab7 (G) in *Sele*$^{+/+}$ or *Sele*$^{-/-}$ PMs obtained from mice after infection with LM 3 days. 60 cells were analyzed in each group of examination. (Scale bar: 10 μm). (H) Immunoblot analysis of biotin-labeled of membrane IFNγR2, internalized and biotin-labeled proteins (cells stimulated with IFNγ for 30 min) and intracellular proteins after recycling. (I and J) Quantification of the ratio of internalized (I) and (J) recycled IFNγR2 in *Sele*$^{-/-}$ and *Sele*$^{+/+}$ PMs. PM: peritoneal macrophages, SM: splenic macrophages, Endoso: endosome, WCL: whole cell lysis. Data are shown mean ± SD of three independent experiments (right panel of A-G, I and J) or one representative of three independent experiments with similar results. *$p < 0.05$, **$p < 0.01$ (Student's t test).

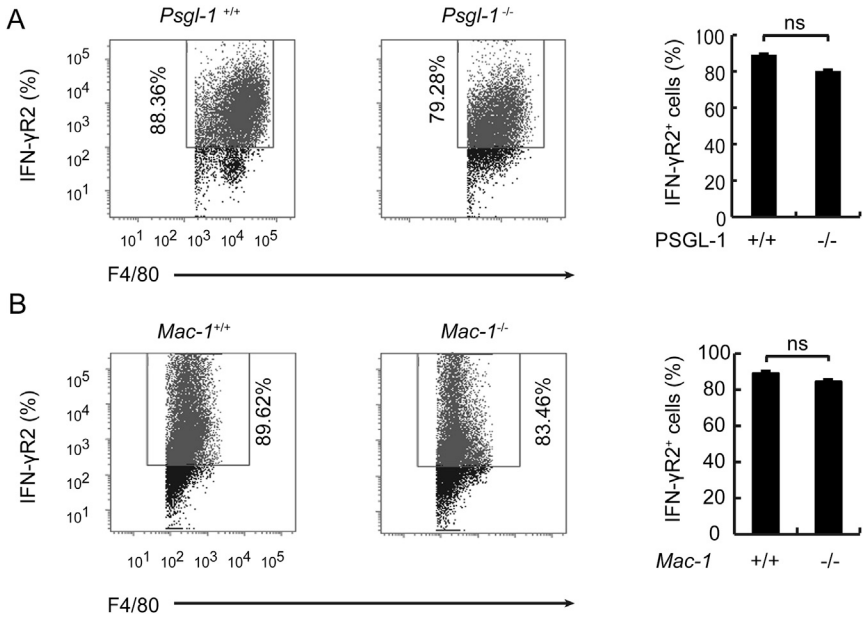

Figure S4. Normal Membrane Expression of IFN-γR2 on Macrophages in *Psgl-1*$^{-/-}$ or *Mac-1*$^{-/-}$ Mice Infected with LM, Related to Figure 4

(A, B) Flow cytometry analysis of membrane IFN-γR2 on peritoneal macrophages from *Psgl-1*$^{-/-}$ (A) or *Mac-1*$^{-/-}$ (B) mice infected with LM on day 3. LM: *Listeria monocytogenes*. Data are shown mean ± SD of three independent experiments (right panel of A and B) or one representative of three independent experiments with similar results.

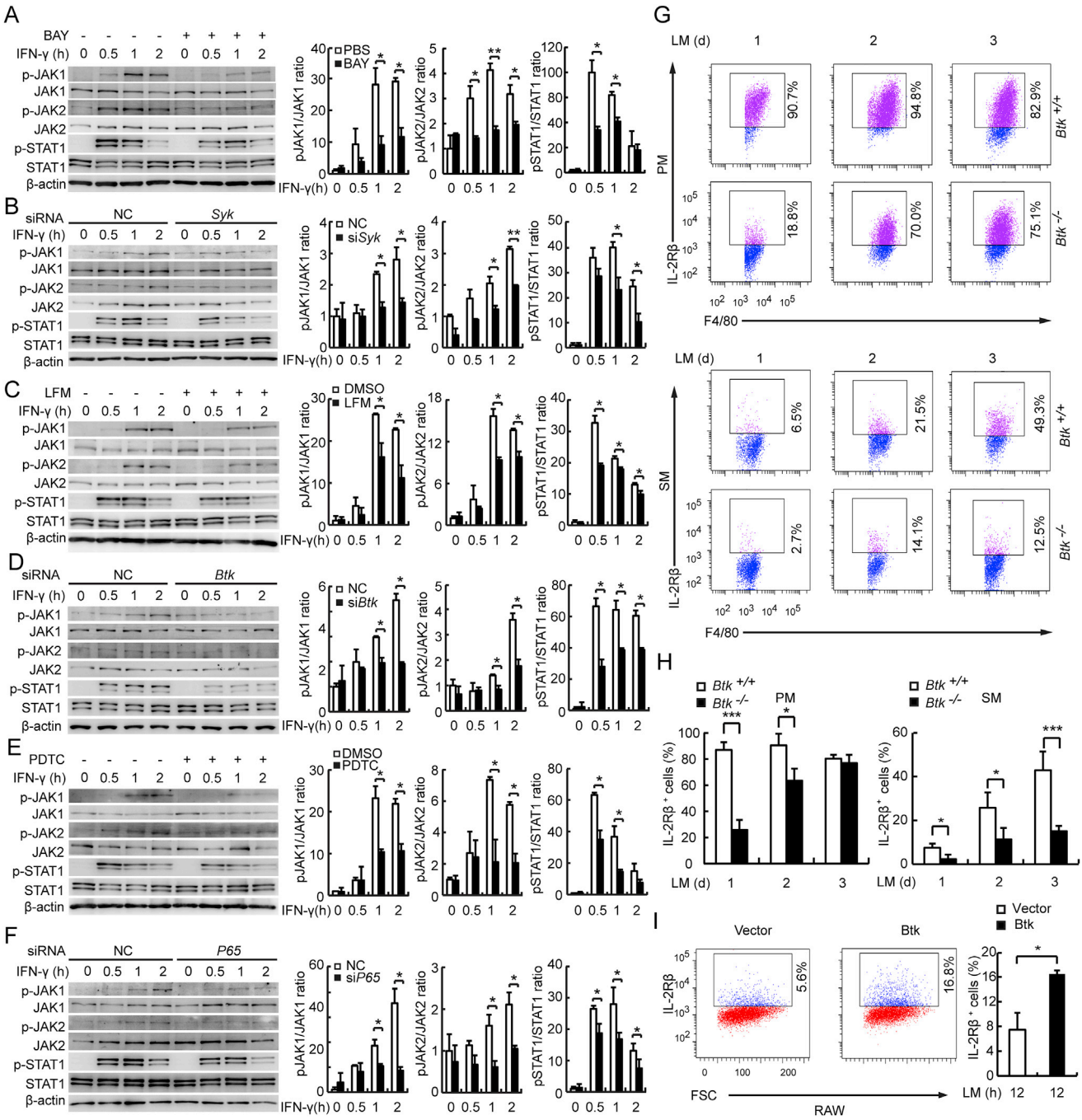

Figure S5. *Btk*$^{-/-}$ Mice Have Decreased IL-2Rβ Expression on the Membrane of Macrophages, Related to Figure 5

(A-F) Representative Immunoblots and quantification of JAK/STAT signaling molecules in the lysates of *Sele*$^{+/+}$ BMDM pretreated with inhibitors or siRNAs and then stimulated with IFN-γ (10U/ml) at indicated times. BAY-61-3606 for SYK: 10 μM (A), siRNA for *Syk* (B); LFM-A13 for BTK: 100 μM (C), siRNA for *Btk* (D); PDTC for P65: 5 μM (E), siRNA for *P65* (F). (G) Flow cytometry analysis of IL-2Rβ subunit expression on peritoneal macrophages or splenic macrophages from *Btk*$^{+/+}$ or *Btk*$^{-/-}$ mice infected with LM for the indicated days. Isotype IgG served as a negative control. (H) Quantification analysis of IL-2Rβ subunit expression on peritoneal macrophages or splenic macrophages of G. (I) Flow cytometry analysis and quantification of IL-2Rβ subunit expression on RAW 264.7 cells stimulated with LM 12 h after transfection with vector or Btk plasmid. PM: peritoneal macrophages, SM: splenic macrophages, LM: *Listeria monocytogenes*, BMDM: bone marrow derived macrophage. Data are shown mean ± SD of three independent experiments (right panel of A-F, H and I) or one representative of three independent experiments with similar results.*$p < 0.01$, ***$p < 0.001$ (Student's t test).

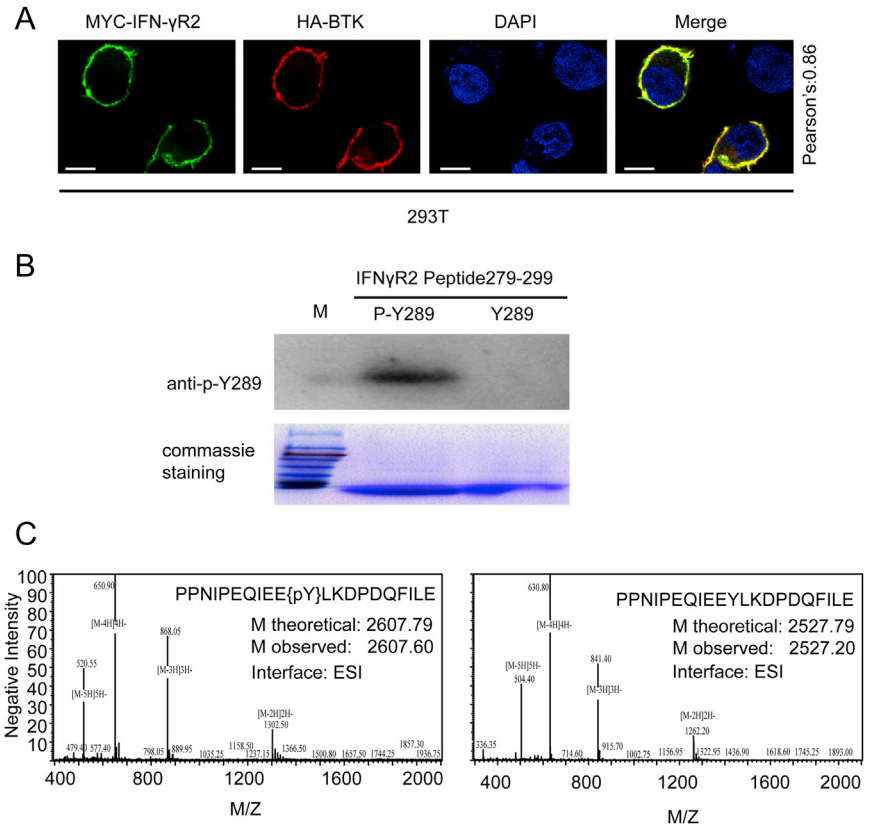

Figure S6. Immunoblot Analysis of the Specificity of Polyclonal Antibody against IFN-γR2 pY289, Related to Figure 6

(A) IFN-γR2 and BTK expression vectors were co-transfected into HEK293T cells, and the location of IFN-γR2 and BTK was determined by confocal microcopy (Scale bar: 10 μm). (B) Examination of binding of polyclonal antibody to p-IFN-γR2 279-299 peptide or IFN-γR2 279-299 peptide by immunoblot analysis (upper panel), and Coomassie staining of the peptides (lower panel). (C) Mass spectrometry analysis of p-IFN-γR2 279-299 peptide or IFN-γR2 279-299 peptide. Data are one representative of three independent experiments with similar results.

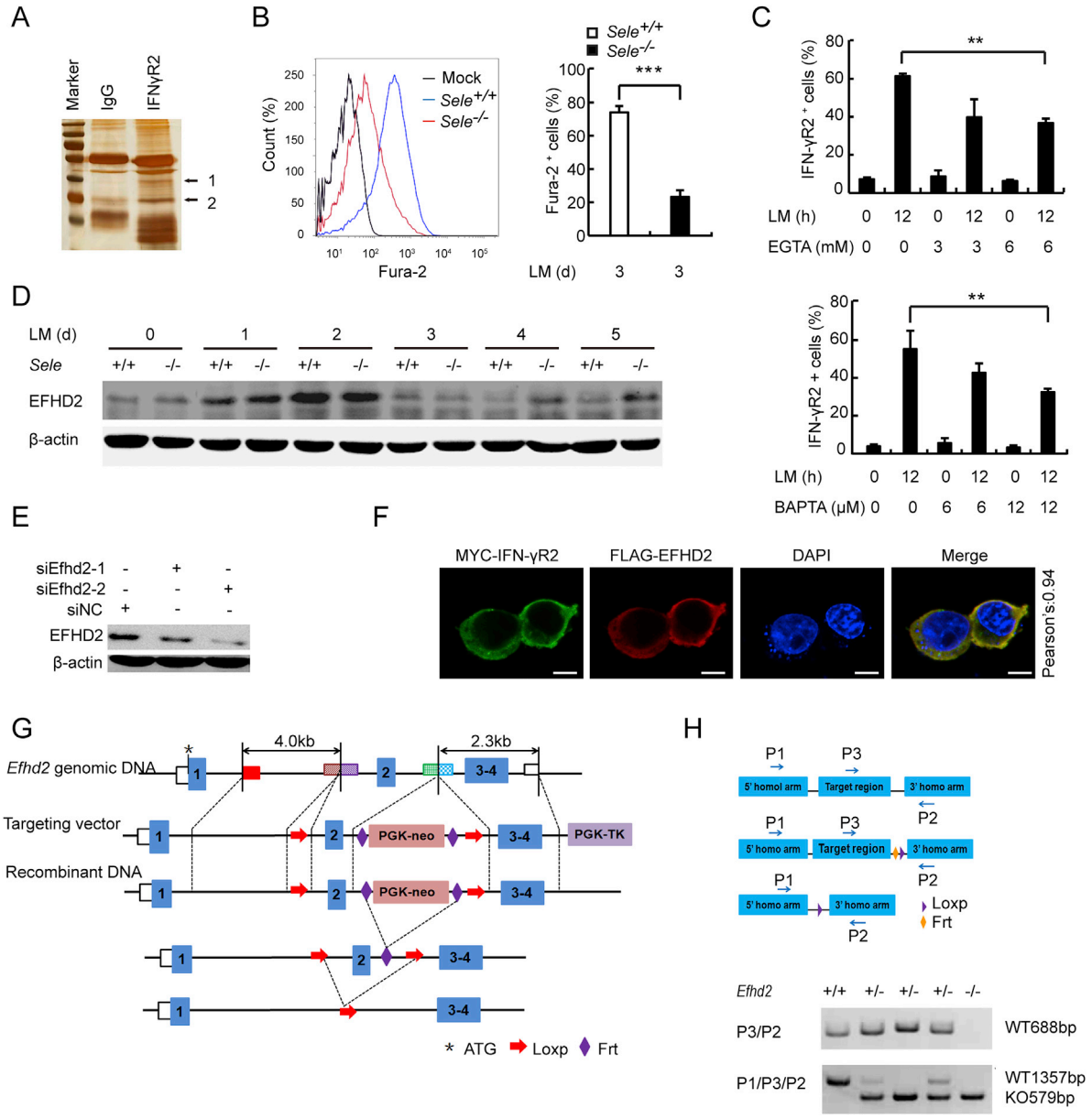

Figure S7. EFhd2 Associates with IFN-γR2 and Generation of EFhd2-Deficient Mice, Related to Figure 7

(A) Silver staining of proteins separated by SDS-PAGE after immunoprecipitation with control IgG or anti-IFN-γR2 antibody. Arrow 1 indicates the location of IFN-γR2, and the band indicated by arrow 2 was analyzed by reverse-phase nanospray liquid chromatography-tandem mass spectrometry. (B) Flow cytometry analysis of intracellular calcium concentration indicated by staining with fura-2 of peritoneal macrophages of *Sele*$^{-/-}$ and *Sele*$^{+/+}$ mice infected with LM *in vivo* for indicated time. (C) Flow cytometry analysis of surface IFN-γR2 on peritoneal macrophages pretreated with EGTA (top panel) and BAPTA-AM (lower panel) for 1 h and then treated with LM *in vitro* for indicated times. (D) Immunoblot analysis of EFhd2 expression in lysates of peritoneal macrophages of *Sele*$^{-/-}$ and *Sele*$^{+/+}$ mice infected with LM indicated times. (E) Western blot analysis of the silencing of *Efhd2* expression in bone marrow-derived macrophages by two *Efhd2*-specific siRNAs targeting either amino acids 320-340 or amino acids 587-607. (F) Confocal microscopy of the co-localization of IFN-γR2 and EFhd2 in HEK293T cells co-transfected with Flag-tagged IFN-γR2 and Myc-tagged EFhd2. (Scale bar: 10 μm). (G) Schematic illustrating the generation and characterization of loxp-flanked *Efhd2* conditional knockout mice. (H) The strategy for genotype identification (upper panel). PCR analysis was performed to identify the genotype of the mice (lower panel). The size of the DNA fragments are indicated in bp on the right side of the gel images, and the primers used for genotyping are indicated on the left. Data are shown mean ± SD of three independent experiments (B and C) or one representative of three independent experiments with similar results. **p < 0.01, ***p < 0.001 (Student's t test).